Physics – Uspekhi **43** (11) 1103 – 1123 (2000)

REVIEWS OF TOPICAL PROBLEMS PACS numbers: 82.40.We, 94.10.Fa

Artificially ionized region as a source of ozone in the stratosphere

A V Gurevich, A G Litvak, A L Vikharev, O A Ivanov, N D Borisov, K F Sergeĭchev

DOI: 10.1070/PU2000v043n11ABEH000684

Contents

Abstract. A set of physical and chemical processes occurring in a microwave stratospheric discharge of nanosecond duration is discussed in connection with the effect they may have locally on the ozone layer in the artificially ionized region (AIR) in the stratosphere. The AIR, to be created at altitudes of 18 – 20 km by the microwave breakdown of air with ground-produced powerful electromagnetic wave beams, is planned for use in the natural physical experiment aimed at active monitoring of the ozone layer (its internal state and a set of plasma-chemical and photochemical processes) by controllably generating a considerable amount of ozone in the stratosphere. Results of relevant theoretical studies are presented, as are those of a large series of laboratory experiments performed under conditions similar to those prevailing in the stratosphere. Discharge regimes securing the efficient growth of ozone concentration are identified and studied in detail. It is demonstrated that such a stratospheric ozonizer is about as efficient as the best ground-based ozonizers used at present. For typical stratospheric conditions (low pressures and temperatures $T \sim 200 - 220$ K), it is shown that the intense generation of ozone in a microwave breakdown effected by groups of short nanosecond pulses does not virtually increase the density of nitrogen oxides — gases that play a vital role in catalytic ozone-decomposing reactions. The possibility of effectively producing ozone in prebreakdown electric fields is established experimentally. It is demonstrated that due to its long lifetime, ozone produced locally at altitudes of 18 – 20 km may spread widely under the action of winds and turbulent diffusion, thus leading to an additional — artificial — ozonization of the stratosphere.

A V Gurevich P N Lebedev Physics Institue, Russian Academy of Sciences
Leninskiĭ prosp. 53, 117924 Moscow, Russian Federation
Tel. (7-095) 132 64 14. E-mail: alex@lpi.ru
A G Litvak, A L Vikharev, O A Ivanov Institute of Applied Physics, Russian Academy of Sciences
ul. Ul'yanova 46, 603600 Nizhniĭ Novgorod, Russian Federation
Tel. (7-8312) 38 45 60. Fax (7-8312) 36 20 61
E-mail: val@appl.sci-nnov.ru
N D Borisov Institute of Terrestrial Magnetism, Ionosphere and Radiowave Propagation, Russian Academy of Sciences
142092 Troitsk, Moscow Region, Russian Federation
Tel. (7-095) 334 09 15. Fax (7-095) 334 01 24
E-mail: borisov@lpi.ru
K F Sergeĭchev General Physics Institute, Russian Academy of Sciences
ul. Vavilova 38, 117942 Moscow, Russian Federation
Tel. (7-095) 132 82 39. Fax (7-095) 135 80 11
E-mail: sergeichev@fpl.gpi.ru

Received 25 July 2000
Uspekhi Fizicheskikh Nauk **170** (11) 1181 – 1202 (2000)
Translated by M V Tsaplina; edited by A Radzig

1. Introduction

Ozone belongs to the minor neutral constituents of the Earth's atmosphere. In spite of the fact that at a certain altitude its maximum concentration is nearly five orders of magnitude lower than that of air molecules, it protects the life on Earth from the destructive effect of ultraviolet (UV) solar radiation. The altitude distribution of ozone is rather nonuniform and shows a clearly pronounced peak at altitudes between 18 and 30 km. The altitude region near the maximum, where the bulk of ozone is concentrated, is called the ozone layer. The ozone distribution over the stratosphere is formed as a result of chemical processes and is affected by a number of factors: the UV radiation of the Sun, large-scale circulation of air in the atmosphere, turbulent diffusion, and the distribution of air temperature in the stratosphere. The influence of the above-mentioned factors is different at

different latitudes, which leads to the latitude dependence of the ozone layer parameters. So, at low latitudes the layer is positioned higher ($H \sim 30$ km) and the maximum ozone concentration in it is larger ($[O_3]_{max} \sim 5 \times 10^{12}$ cm^{-3}) than in the auroral zones where the typical altitude of the maximum is $H = 18-20$ km, and the concentration is $[O_3]_{max} \sim 3 \times 10^{12}$ cm^{-3} [1, 2].

It should be emphasized that the integral absorption of the UV solar radiation by ozone depends on the wavelength (it is maximum when $\lambda \sim 255$ nm) and grows exponentially with increasing ozone concentration in the layer. Hence, even a slight decrease of the total ozone content may lead to a strong change in the UV radiation intensity on the Earth. So, when the ozone content decreases by only 10%, the radiation intensity on the Earth increases 50-fold for $\lambda = 288$ nm, 6-fold for $\lambda = 293$ nm and only 1.6-fold for $\lambda = 302$ nm [3]. This exceedingly important feature is precisely what has drawn the heightened attention of scientists and the world community to the analysis of the state of the ozone layer.

Observation of the ozone layer shows that the ozone concentration in it changes not only with latitude, but also from season to season and from year to year. A considerable ozone depletion, called the 'ozone hole' [2 – 5], was revealed in the spring of 1985 over the Antarctic Continent. Further observations in the Antarctic stratosphere revealed the rather complicated dynamics of the 'ozone hole'. At the early stage of observation (1985 – 1987), its area continuously expanded and its duration of presence became longer, which caused certain concern. Later on, however, the character of its transformation became much less definite, and the dynamics of the 'ozone hole' over the Antarctic Continent still remain not quite clear.

A noticeable contribution to the decrease of ozone concentration is thought to be in particular of anthropogenic nature. This effect may heighten, which arouses natural concern about the fate of the ozone layer. H Johnston and P Krutzen were the first to express their apprehension in the early 1970s and to draw attention to the atmospheric pollution by nitric oxides released due to stratospheric aviation [6, 7]. After that, in addition to the nitrogen catalytic cycle, chlorine (due to Freon decomposition) and hydrogen catalytic cycles also leading to ozone depletion were revealed. This impelled the world community to take some measures directed to limit the production of substances that have a negative effect on the ozone layer. The Vienna Convention on ozone layer protection was adopted in 1985, and the Montreal Protocol according to which the participant countries are to curtail sharply the production of long-lived Freons and other ozone-decomposing substances was signed in 1987.

However, the answer to the question of the necessity and sufficiency of these measures now remains vague. The point is that the observation of the state of the ozone layer from the viewpoint of the anthropogenic effect has no reliable predictive force owing to the possibility of long-lived minor impurities of catalytic products existing in the atmosphere and poor control over their release into the atmosphere. Alternatively, a theoretical description of the influence of minor impurities upon the ozone layer is fairly difficult. First of all, several hundred equations describing the chain of chemical reactions should simultaneously be considered, and not all the rate coefficients for the reactions are well known. If, in addition, the influence of ultraviolet solar radiation, atmospheric winds, turbulence, and stratospheric clouds with their complex heterogeneous reactions proceeding with the participation of nitrogen- and chlorine-containing compounds [2] are taken into account, it becomes clear that purely theoretical calculations cannot be a source of reasonably reliable predictions of ozone layer behavior. It is not accidental that, in particular, neither the predictions by Johnston and Krutzen concerning a substantial lowering of ozone concentration in the stratosphere by the late 1980s nor the predictions, following from the observations by Farman et al. [8], of catastrophic consequences of the increasing Antarctic 'ozone hole' were justified.

It is quite obvious that permanent and controllable physical experiments in the stratosphere are necessary to make a reliable judgment of the effect of minor impurities on the behavior of such a complex system. The present review is devoted to the feasibility of such experiments at the current stage. It is advised that the experimental research will be carried out using an artificially ionized region (AIR) created in the stratosphere by means of pulsed microwave breakdown in crossed powerful electromagnetic wave beams produced on the ground. The microwave radiation parameters necessary to create an AIR can be evaluated using the results of investigations of gas discharges in wave beams. An extensive programme of experimental and theoretical research of such a discharge, stimulated by advances in the design of high-power microwave radiation sources (gyrotrons [9] and relativistic electron beam generators [10]), was performed in the 1980s in the USSR and USA [11 – 18]. The idea of creating an AIR well reflecting radio waves (a radio mirror) and exploiting it for tele- and radio communication was suggested as far back as the early 1980s by A V Gurevich [19] and was further developed in Refs [20, 21]. To maintain a radio mirror in the crossing region of the two wave beams, the following microwave radiation parameters were proposed: a wavelength of 5 – 100 cm, pulse duration of 1 – 10 ns, and pulse repetition rate of $10^4 - 10^5$ Hz. A high pulse repetition rate is necessary in order that the decrease in the plasma density between pulses due to deionization be small and a high mean electron concentration be maintained. It should be noted that the possible ecological consequences of the creation and long-term maintenance of a radio mirror were discussed at length in papers [22 – 25]. The results of this discussion lay a good basis for our analysis of the effect of a nanosecond microwave discharge upon the ozone concentration in the stratosphere. It is precisely the use of short nanosecond microwave pulses and the low gaseous temperature in the stratosphere that determine the absence in our case of the negative ecological effects discussed in those papers.

The review is organized as follows. Section 2 is devoted to the theory of AIR creation in the stratosphere, the study of the related physical processes, the investigation of ionized region stability, and the laboratory simulation experiments on the creation and maintenance of an AIR in crossed microwave beams. The section to follow analyzes the plasma-chemical processes under the conditions of a nanosecond microwave discharge in the air. The results of numerical calculations describing the kinetics of minor neutral components in an AIR are presented. The section is mainly devoted to the results of laboratory experiments in which the ozone concentration dynamics are examined. It is demonstrated that depending on the microwave oscillator operation regime and conditions in the discharge the concentrations of both ozone and ozone-destructive nitric oxides NO and NO_2 may increase. The conditions are revealed and thoroughly investigated under which an appreciable ozone production is

observed, whereas the NO and NO_2 concentrations remain, in fact, at the level of the background values. An efficient increase of the ozone concentration in a microwave resonator in prebreakdown electric fields was also observed. The possibility of using AIR in an environmental experiment exploring the effect upon the ozone layer in the stratosphere is considered in Section 4 on the basis of the results of laboratory experiments and numerical calculations. The methods of remote ground-based diagnostics of the plasma-chemical processes in an AIR, associated with the dynamics of minor neutral components (ozone in the first place) are scrutinized. The expenditure of energy and the optimum conditions for an efficient ozone production are estimated. The possibility of replenishing a sufficiently vast area in the stratosphere with artificially generated ozone is discussed.

2. An artificially ionized region in the atmosphere

2.1 Schematic of AIR creation

The scheme of a proposed realization of the environmental experiment is presented in Fig. 1. Two powerful electromagnetic wave beams with frequencies of 10–40 GHz are sent to the atmosphere with the help of ground-based antennas. In the beam crossing region at altitudes $H = 20-30$ km, where the electric field is particularly large, a gas discharge is set up, i.e. an AIR is formed which, the same as a discharge in the ozonizer, will be an efficient ozone source. In the AIR, plasma electrons acquire energy from the electric field and cause oxygen molecule dissociation, and then the oxygen atoms are converted into ozone. This plasma-chemical method of ozone production is especially efficient with pulsed electric discharges of short duration and a high repetition rate [26].

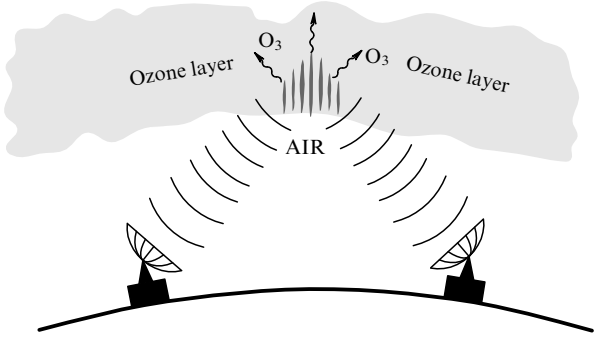

Figure 1. Schematic of AIR formation.

In the schematic diagram of the experiment in Fig. 1, for air ionization within nanosecond intervals the electric fields in the beams should be strong. Estimates show that for AIR formation in the three-centimeter wavelength region at an altitude $H = 30$ km with the help of antennas of 100 m in diameter and located at a distance of 30 km from one another, the pulse power in the wave beams should exceed the value $P = 4 \times 10^9$ W for a pulse duration $\tau = 50$ ns. This power level has already been reached on contemporary microwave oscillators in laboratory experiments. Thus, the creation of an atmospheric microwave discharge appears to be quite feasible with the modern state of technology.

Notice that to form an AIR at altitudes of several tens of kilometers, crossed beams are more practicable than a single electromagnetic wave beam. For moderate transmitting antenna parameters (with a diameter of several tens of meters), the convergence angle for a single beam is exceedingly small ($\Theta = 10^{-3}$) and the maximum electron concentration N_{em} in a discharge in a single beam appears to be not high: $N_{em} = N_{cr}\Theta^2$ [16], where

$$N_{cr} = \frac{m(\omega^2 + \nu_c^2)}{4\pi e^2}$$

is the critical electron concentration for the frequency ω of incident microwave radiation. The value of N_{em} is insufficient to attain a considerable atomic oxygen concentration within a short microwave pulse. In crossed beams, much higher N_e values can in principle be reached and controllable variation of the AIR position in space can be provided. Figure 2a presents the general scheme of electrical breakdown in crossed beams, and Fig. 2b shows the beam intersection region, where the heavy lines correspond to antinodes due to the interference of coherent fields. We henceforth assume an AIR to be formed in crossed wave beams.

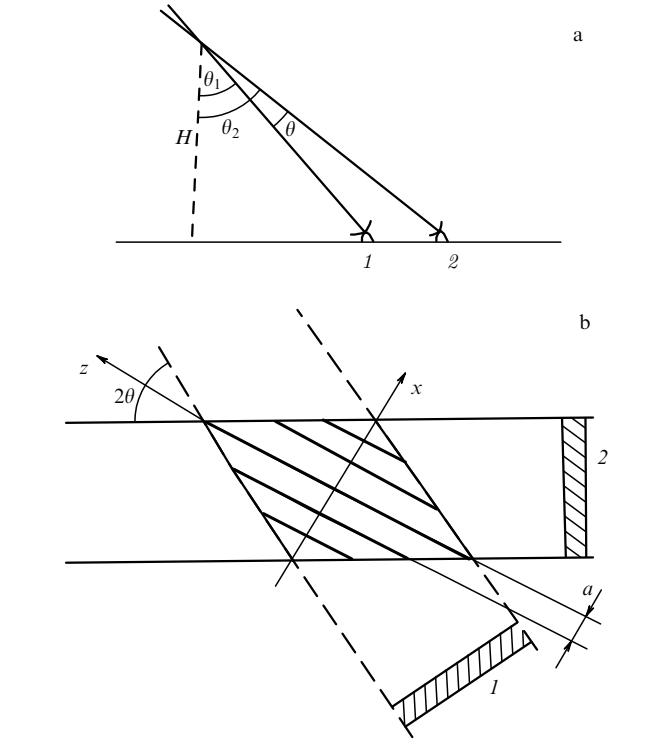

Figure 2. Schematic of breakdown in crossed beams (a) and the beam intersection region (b). Figures *1* and *2* indicate pulses radiated by transmitters.

2.2 Pulsed microwave breakdown of air

When affected by a strong high-frequency electric field, electrons acquire considerable energy sufficient to ionize neutral molecules of the air. In alternating electric fields with amplitudes exceeding the critical breakdown field strength E_{cr}, the electron concentration begins to rise with time in the form of an avalanche and a breakdown occurs. Many experimental and theoretical papers have been devoted to the study of breakdown in the air. We shall present here the result of the recent theoretical calculation of the field E_{cr} (in

kV cm^{-1}), which agrees well with observations and is based on the kinetic theory of electron behavior in strong electromagnetic fields [21]:

$$E_{\rm cr} = 28.2C\left(\frac{\nu_{\rm c}}{\omega}\right)\frac{N_{\rm m}}{2.7\times 10^{19}\ {\rm cm}^{-3}}\left(1+\frac{\omega^2}{\nu_{\rm c}^2}\right)^{1/2}. \qquad (1)$$

Here $\nu_{\rm c} = 1.7(N_{\rm m}/10^7\ {\rm cm}^{-3})\ {\rm s}^{-1}$ is the characteristic electron–molecule collision frequency, $N_{\rm m}$ is the air molecule concentration in cm^{-3}, $C(\nu_{\rm c}/\omega)$ is a coefficient of the order of unity, and ω is the cyclic frequency of the microwave field.

From Eqn (1) it follows that the critical field of a high-frequency breakdown decreases rapidly (proportionally to the concentration) with altitude until the collision frequency $\nu_{\rm c}$ becomes of the order of the wave frequency ω. With a further rise of the altitude, the critical field remains constant: $E_{\rm cr} \simeq 6.1(\omega/10^{12})$ kV cm^{-1}.

In above-critical fields $E > E_{\rm cr}$, the growth of the electron number density with time is characterized by the difference of electron ionization frequency $\nu_{\rm i}$ and electron attachment frequency $\nu_{\rm am}$ to oxygen molecules, where $\nu_{\rm am} \simeq 7.6(N_{\rm m}/10^{13}\ {\rm cm}^{-3})\ {\rm s}^{-1}$ is the maximum frequency of dissociative electron attachment during a breakdown pulse. The approximate analytical formula for the air ionization frequency by electron impact has the form [21]

$$\frac{\nu_{\rm i}}{\nu_{\rm am}} = F\left(\frac{E}{E_{\rm cr}}\right)\left(\frac{E}{E_{\rm cr}}\right)^2 C_1\left(\frac{\omega}{\nu_{\rm c}}\right)\exp\left\{-4.7\left[C_2\left(\frac{\omega}{\nu_{\rm c}}\right)\frac{E_{\rm cr}}{E}-1\right]\right\}. \qquad (2)$$

Here, $F(x) = (2/3)[1 + 6.3\exp(-2.6/x)]$ and the coefficients $C_1(\omega/\nu_{\rm c})$, $C_2(\omega/\nu_{\rm c})$ are close to unity and depend rather weakly on their arguments. In particular, the coefficient C_2 changes monotonically from 1.0 for $\omega/\nu_{\rm c} \ll 1$ to 1.1 for $\omega/\nu_{\rm c} \gg 1$.

For a comparatively weak supercriticality, the ionization frequency variation with field as in Eqn (2) can be approximated by the power-law dependence

$$\nu_{\rm i} = \nu_{\rm am}\left(\frac{E}{E_{\rm cr}}\right)^{\alpha}, \qquad (3)$$

where $\alpha \simeq 5.3$ for the interval $1 \ll E/E_{\rm cr} \leqslant 3$. One can see that the ionization frequency grows very rapidly with increasing field amplitude. For large fields ($E/E_{\rm cr} \geqslant 4$), the ionization frequency growth becomes slower ($\alpha \leqslant 2$). Owing to field interference, the most significant ionization in crossed radio wave beams is only possible, according to Eqn (3), in narrow layers corresponding to field antinodes.

It is of interest to find the optimum ionization conditions when for a given energy of a high-frequency pulse the number of free electrons occurring in the air reaches its maximum. On the one hand, the energy W of the pulse is proportional to its duration τ and to the field amplitude squared $|E|^2$:

$$W = C_0|E|^2\tau, \qquad (4)$$

where C_0 is a constant. On the other hand, the number of pulse-induced free electrons for $E > E_{\rm cr}$ is equal to

$$N_{\rm e} = N_{\rm e0}\exp\left[\nu_{\rm i}(E)\tau\right]. \qquad (5)$$

According to Eqns (4), (5), the pulse energy W necessary for creating the electron number density $N_{\rm e}$ is specified by the function $\chi(E/E_{\rm cr})$ [21]:

$$\chi\left(\frac{E}{E_{\rm cr}}\right) = \frac{\nu_{\rm i}(E/E_{\rm cr})}{\nu_{\rm am}}\left(\frac{E_{\rm cr}}{E}\right)^2. \qquad (6)$$

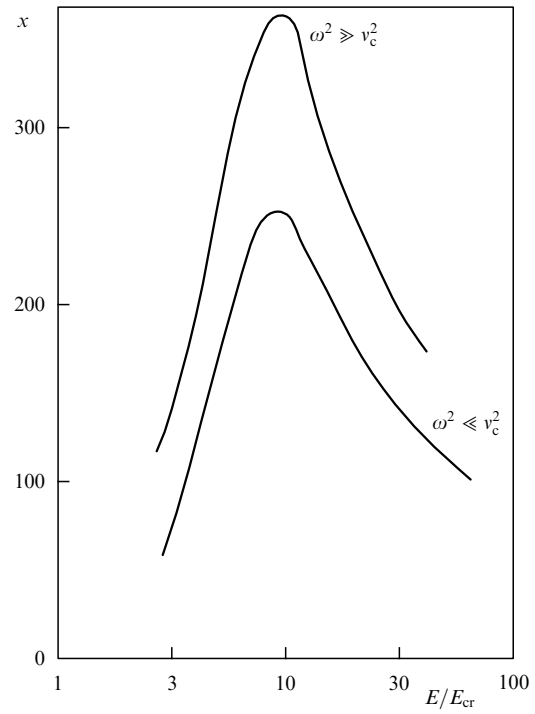

Figure 3. Dependence of the function χ on $E/E_{\rm cr}$.

The optimum ionization condition, i.e. the minimum expenditure of energy corresponds to the maximum of the function $\chi(E/E_{\rm cr})$, which is attained provided that

$$E \simeq (5-7)E_{\rm cr}, \qquad \omega \simeq \nu_{\rm c}. \qquad (7)$$

Figure 3 demonstrates the behavior of the function $\chi(E/E_{\rm cr})$ for two limiting ratios of the wave frequency ω to the collision frequency $\nu_{\rm c}$: $\omega/\nu_{\rm c} \gg 1$ and $\omega/\nu_{\rm c} \ll 1$. In both cases, a sharp peak exists which corresponds to the optimum conditions. Table 1 presents the values of the critical field $E_{\rm cr}$ for the optimum conditions $\omega = \nu_{\rm c}$ at altitudes of 20 and 30 km.

Table 1

H, km	$N_{\rm m}$, cm^{-3}	$\nu_{\rm c}$, cm^{-1}	$\lambda_{\rm op}$, cm	$E_{\rm cr}^{\rm op}$, kV cm^{-1}
20	1.8×10^{18}	3.1×10^{11}	0.6	3.25
30	3.7×10^{17}	5.9×10^{10}	3.2	0.62

2.3 Ionization relaxation

In the wave beam crossing region, the velocity distribution function of electrons differs strongly from Maxwellian during the action of a microwave pulse. At the end of the pulse, the electron distribution relaxes to equilibrium and, moreover, the plasma density in the AIR lowers owing to various loss mechanisms (recombination, attachment, atmospheric wind, and diffusion).

In the course of relaxation, the electron distribution function is at first symmetrized very rapidly (within times $\Delta t \sim 10^{-11}-10^{-12}$ s), i.e. becomes dependent on time and energy only. Then the relaxation of the energy distribution function proceeds slower, the characteristic relaxation time

being different for different energy ranges ε. In the low-energy range, $\varepsilon \leqslant 1-2$ eV, when characterizing the mean electron energy, one can approximately speak of the electron temperature T_e. The electron temperature relaxation time at low energies is

$$\tau_T = \left[\delta(T_e)\nu(T_e)\right]^{-1}, \quad (8)$$

where $\nu(T_e)$ is the effective electron–molecule collision frequency, and $\delta(T_e)$ is the mean fraction of the electron energy lost in a collision. For energies $\varepsilon \leqslant 1$ eV, one may assume $\delta \simeq (1-2) \times 10^{-3}$. The complete electron temperature relaxation for altitudes $H = 20-30$ km is reached within the time $\tau_T = (0.6-3) \times 10^{-6}$ s.

In the energy range $2 < \varepsilon < 5$ eV, the leading role in the relaxation is played by inelastic collisions between electrons and neutral molecules. The relaxation constitutes a gradual displacement of the distribution towards the lower-energy range. The characteristic relaxation time is $\tau_\varepsilon \sim 10^{-9}(N_m/10^{17}\,\mathrm{cm}^{-3})^{-1}$ s, i.e. $\tau_\varepsilon = (0.6-3) \times 10^{-10}$ s for $H = 20-30$ km. For higher energies, $6 < \varepsilon < 12$ eV, the relaxation rate is nearly the same.

The temperature relaxation time is very short, much shorter than the ionization relaxation time. Therefore, for characteristic times exceeding τ_T the electron temperature may be assumed to be close to the molecular temperature, and the ionization relaxation can be described within the hydrodynamic approximation. The electron number density variation can in this case be given by the particle balance equation

$$\frac{\partial N_e}{\partial t} = D_a \Delta N_e - \mathbf{v}\nabla N_e - N_e \sum_j \alpha_{ij} N_i^{(j)} - \nu_{aT} N_e\,. \quad (9)$$

Here D_a is the ambipolar diffusion coefficient, $\mathbf{v}$ is the atmospheric wind velocity, α_{ij} are the recombination coefficients for various processes, $N_i^{(j)}$ is the j-kind ion number density, and ν_{aT} is the attachment coefficient for triple collisions. For ν_{aT}, the expression [21]

$$\nu_{aT} = 8.3 \times 10^2 \left(\frac{N_m}{10^{17}}\right)^2 \left\{\frac{300}{T}\exp\left[-\frac{2(1-T/300)}{T/300}\right] + 0.2\right\} \quad (10)$$

holds, where T is the air temperature in kelvins, and ν_{aT} is measured in s^{-1} units.

The relative role of various loss mechanisms in the course of ionization relaxation depends on the electron concentration in the ionized region, its size and the altitude of its formation. When the air is ionized by a small group of short pulses for typical region sizes L_z and L_x (see Table 2) and wind velocity $v \geqslant 1$ m s^{-1}, the diffusion and the ionization product entrainment in the period between two pulses can be neglected. Recombination may play a significant role only at the early stage of relaxation in the case of a high maximum plasma concentration. Hence, the ionization relaxation time can be estimated to a first approximation as $\tau_r \approx \nu_{aT}^{-1}$.

Table 2

H, km	λ, cm	L_z, m	L_x, m	N_{em}, cm^{-3}
20	0.8	4	3	5×10^{12}
	3	15	11	10^{12}
30	0.8	7	4	2×10^{12}
	3	27	13	2×10^{11}

2.4 Laboratory studies of a discharge in crossed wave beams

In recent years, along with the theoretical studies, a cycle of laboratory experiments [27–29] has been carried out to examine the dynamics and structure of a self-sustained microwave discharge in crossed wave beams. A gyrotron with an 8-mm wavelength range was used as a radiation source providing sufficiently high pulse power and pulse duration values, which made a breakdown feasible and allowed some stages of post-breakdown discharge evolution to be observed over a wide air density range corresponding to altitudes of 15–50 km.

The experiments were carried out according to the scheme depicted in Fig. 4. The microwave radiation of the gyrotron was converted into a Gaussian beam of linearly polarized electromagnetic waves with the aid of a transducer and was directed inside the anechoic vacuum chamber. On passing through a dielectric lens, the wave beam split up into two equal-power beams which, when reflected from the metallic mirrors, crossed in the central region of the vacuum chamber. The experimental conditions were as follows: the wavelength was $\lambda = 8$ mm, the pulse duration $\tau = 4-55$ μs, the pulse power in each beam $P = 100$ kW, the air pressure in the vacuum chamber $p = 0.3-70$ Torr, the angle between the beam axes $2\theta = 60°$, and the beam diameter in the crossing region (by the level of e-time fall of intensity) $d = 3$ cm, with the parallel electric field vectors on the axes of both beams. The breakdown conditions were met only in the beam crossing region, where the beam fields were superposed. The first bare electrons necessary for the onset of breakdown were produced by the UV radiation of a spark gap positioned near the breakdown region.

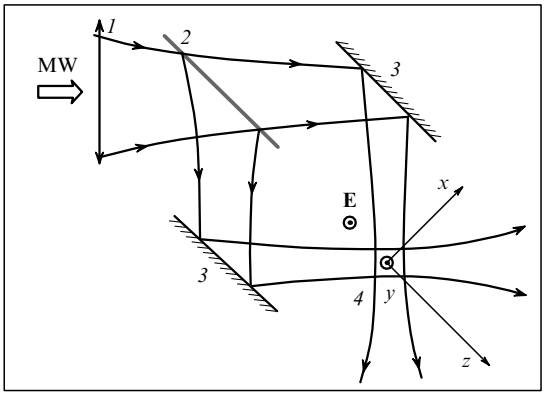

Figure 4. Schematic of the laboratory experiment: *1* — radio lens, *2* — half-mirror, *3* — reflectors, *4* — beam crossing region.

The picture of the discharge was taken in two perpendicular projections: onto the plane formed by the wave vectors of both beams (plane H), and onto the plane bisecting the angle between them (plane E). Two types of photography were employed: integral photography, with the time of exposure exceeding the discharge glow time in each pulse, and high-speed photography using devices based on electron-optical converters in frame and chronographic regimes.

The analysis of the data obtained suggests the following structure and the dynamics of the discharge. During the whole microwave pulse, the discharge is localized in the vicinity of the electric field antinodes (at the maxima of the interference picture occurring in the two-beams superposition

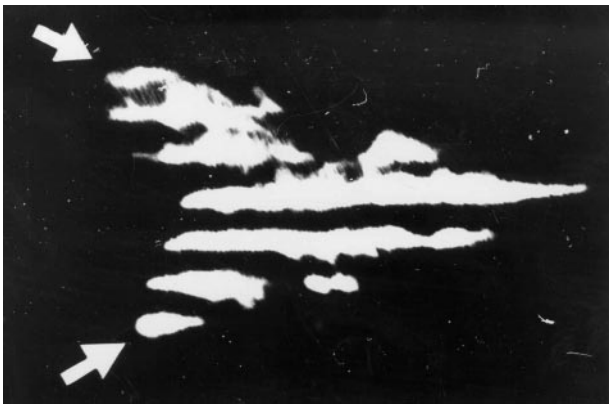

Figure 5. Integral picture of the discharge in the plane of intersection of two beams ($p = 30$ Torr, the arrows indicate the direction of incident radiation).

region). This is illustrated in Fig. 5 by the integral photograph of the discharge in the H plane. Here, the interval between the bright longitudinal strips corresponds to the antinode spacing $\lambda/2 \sin\theta = 8$ mm.

In each ionized layer formed by the field antinode (in the E plane), depending on the air pressure one of the following three types of discharge structure is realized: (1) a quasi-homogeneous (diffusive) discharge at low pressures of 0.3 – 3 Torr or at higher pressures at the early post-breakdown stage of discharge; (2) a laminar discharge with strata perpendicular to the electric field vector, in the pressure range of 3 – 40 Torr, and (3) a discharge fragmented into filaments parallel to the electric field vector, in the pressure range of 40 – 70 Torr. The typical integral photographs in the E plane, corresponding to the three above-listed structures, are given in Fig. 6 (to avoid superposition of glows from different antinodes, which hamper the analysis of the structures in the E plane, the radiation power when taking photos was lowered to a level providing development of the discharge in only one antinode).

As was established, both types of observed discharge fragmentation begin against an initially quasi-homogeneous background (Fig. 6a) and are due to the development of various small-scale ionization instabilities in the discharge plasma. The lamination in the direction of the electric field vector (Fig. 6b) is caused by the plasma-resonant instability [30], and the formation of filament-like plasmoids extended in the direction of the electric field (Fig. 6c) is explained by the development of an ionization-overheating instability which plays a predominant role in the pressure range where $\nu \geqslant \omega$ [31].

The results of the experiments, along with the available theoretical concepts [31 – 34], allow us to predict that in an AIR formed by short (nanosecond) pulses at altitudes of 15 – 50 km, small-scale ionization instabilities will not have time to develop and the AIR structure in different planes will correspond to the integral pictures presented in Figs 5 and 6a. As distinct from laboratory experiments, the wave beams in natural conditions will be much wider, and therefore the number of antinodes occupied by a discharge will be several hundred.

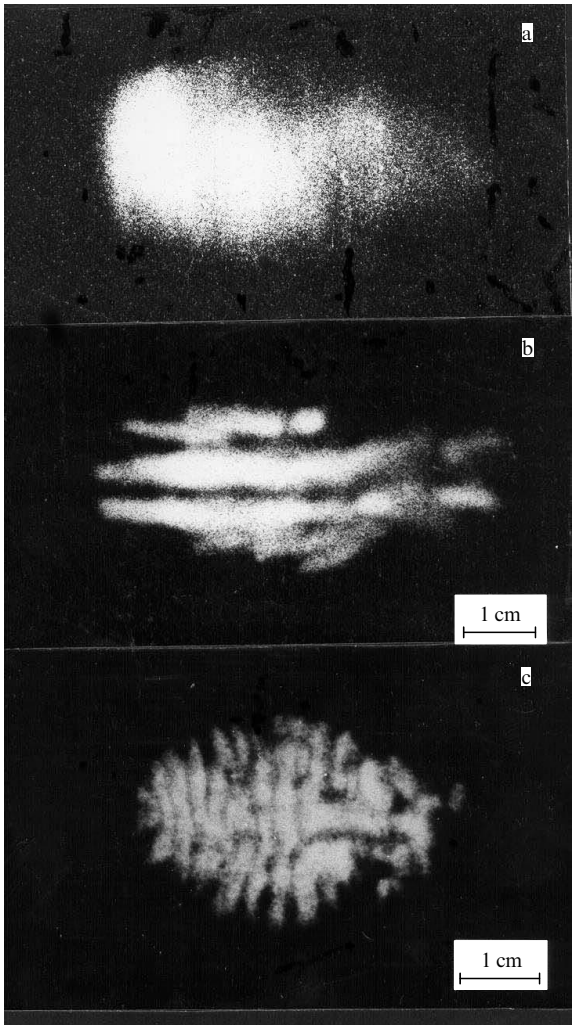

Figure 6. Pictures of the main types of the discharge structure in the plane perpendicular to the plane of beam intersection: (a) $p = 1$ Torr; (b) $p = 10$ Torr, and (c) $p = 70$ Torr. The energy flux is aligned rightward, and the electric field vector is vertical.

2.5 Estimation of atmospheric AIR parameters

We shall estimate the typical AIR parameters and the performance characteristics corresponding to ground-based system for AIR creation at altitudes $H = 20$ and 30 km. Suppose that two coherent microwave beams are used (see Fig. 2). The two ground antennas are at a distance of 30 km from each other. Table 2 gives the linear dimensions L_z and L_x of the ionized region and the maximum electron concentration N_{em} in the central layer, which is determined according to the data of Refs [28 – 33]. Table 3 presents the

Table 3

H, km	D, m	τ_0, ns	T_n, s	λ, cm	E_{cr}, kV cm^{-1}	E_0, kV cm^{-1}	P, GW	W, J
20	100	5	1.2×10^{-3}	0.8	2.4	12	4	20
				3	1.9	9.5	38	190
30	100	24	2.8×10^{-2}	0.8	1.5	7.5	3	70
				3	0.55	2.7	5.5	130

characteristic parameters of the ground-based AIR creation system: D is the antenna diameter, $\tau_0 = \ln(N_{em}/N_{e0})/\nu_i(E_0)$ is the pulse duration necessary for a microwave breakdown under the optimum condition (7), $E = 5E_{cr}$, E_{cr} is the critical field (1), E_0 is the initial electric field in the AIR, P is the pulse power in the wave beam, W is the pulse energy, and T_n is the repetition period for a pulse or a group of ionizing pulses. The calculations were done for two wavelengths $\lambda = 3$ and 0.8 cm.

3. Plasma-chemical processes in microwave discharges

3.1 The principal channels of ozone production and oxygen dissociation

Let us consider the basic processes induced by a microwave discharge and leading to oxygen molecule dissociation and ozone generation in the air. A microwave discharge is responsible for oxygen atom production in several processes, among them the dissociation by electron impact:

$$O_2 + e \rightarrow O + O + e\,, \tag{11}$$

the interaction with electron-excited nitrogen molecules N_2^*:

$$O_2 + N_2^* \rightarrow O + O + N_2\,, \tag{12}$$

and the dissociative electron attachment to oxygen molecules:

$$O_2 + e \rightarrow O^- + O\,. \tag{13}$$

It is a known fact [1, 25] that reactions (11) and (12) are the main sources of atomic oxygen. Reaction (13) makes, on the contrary, a relatively small contribution to the oxygen atom production [23].

Electron-excited nitrogen molecules are produced in a discharge plasma in reactions of molecular excitation by electron impact:

$$N_2 + e \rightarrow N_2^* + e\,. \tag{14}$$

The number of oxygen atoms which can be produced in reactions (12) is determined by both the total number of excitation events (14) and the relation between the oxygen dissociation processes on collisions with excited nitrogen molecules (12) and other excitation relaxation channels. Along with process (12), important channels of the decrease in the number of electron-excited nitrogen molecules are quenching reactions upon their collisions with molecules, which do not lead to oxygen dissociation, and spontaneous emission:

$$N_2^* + M \rightarrow N_2 + \text{products}\,,$$

$$N_2^{**} \rightarrow N_2^* + h\nu\,. \tag{15}$$

The estimates show that the reactions of mutual quenching of the metastable level $A^3\Sigma_u^+$ [35]:

$$N_2(A^3\Sigma_u^+) + N_2(A^3\Sigma_u^+) \rightarrow N_2(C^3\Pi_u) + N_2\,, \tag{16}$$

of the interaction with atomic oxygen:

$$N_2(A^3\Sigma_u^+) + O \rightarrow NO + N\,, \tag{17}$$

and quenching by collisions with electrons:

$$N_2^* + e \rightarrow N_2 + e \tag{18}$$

contribute little to the total loss of electron-excited nitrogen molecules.

We shall point out an important feature of reactions (12) and (15). They are all linear with respect to the excited nitrogen molecules. Consequently, the number of oxygen atoms produced in reactions (12) can be represented as a linear combination of the number of excited particles produced in reactions (14). The total number of excited particles can in turn be found through the rate of the corresponding reaction (14) by integration over the microwave pulse time and over the plasma volume:

$$\sum N_j^* = \int_V \int k_j N_e[N_2]\,dt\,dv\,, \tag{19}$$

where $\sum N_j^*$ is the total number of particles of kind j, k_j the rate constant of excitation in reaction (14), and $[N_2]$ the nitrogen molecule concentration. With allowance for the dissociation processes (11), the total number of oxygen atoms produced in a discharge can be obtained from the relation

$$\sum [O] = \int_V \left[\sum_j C_j \int k_j N_e[N_2]\,dt + 2\int k_d N_e[O_2]\,dt\right] dv\,. \tag{20}$$

Here, k_d is the rate constant of process (11), and C_j are the coefficients which can be determined from the relationship between the collision frequencies in reactions (12) and (15).

It is thus apparent that the number of ozone molecules produced in a microwave discharge is determined by the total number of oxygen atoms, which in turn depends on the rate constants of dissociation (11) and excitation (14) of molecules by electron impact. The rate constants of these reactions are rapidly increasing functions of the parameter E_{eff}/N_m (where $E_{eff} = |E|/(1 + \omega^2/\nu_c^2)^{1/2}$ is the effective electric field strength). Accordingly, the energy cost of the production of one ozone molecule is determined by the expenditure of energy for oxygen dissociation and substantially depends on the electric field dynamics and the electron concentration in the plasma.

The above-discussed kinetic processes responsible for atomic oxygen production in a discharge plasma constitute the first stage of the entire process of ozone generation in an AIR. At the second stage, atomic oxygen undergoes conversion into ozone in the three-particle process

$$O + O_2 + M \rightarrow O_3 + M\,, \tag{21}$$

for which the reaction rate constant is equal to $k_1 = 6.2\times 10^{-34}(300/T)^2$ cm^6 s^{-1} for $M = N_2$, and $k_1 = 6.9\times 10^{-34}(300/T)^{1.25}$ cm^6 s^{-1} for $M = O_2$. The remainder of the atoms are again bound to form oxygen molecules:

$$O + O + M \rightarrow O_2 + M\,. \tag{22}$$

The oxygen atoms simultaneously participate in ozone decomposition in a relatively slow reaction

$$O + O_3 \rightarrow O_2 + O_2\,,$$

$$k_2 = 1.8 \times 10^{-11} \exp\left(-\frac{2300}{T}\right) \text{cm}^3\,\text{s}^{-1}\,. \tag{23}$$

This and other backward reactions of ozone decomposition depend on how much the concentrations of minor constituents of the atmosphere changed as a result of AIR formation or maintenance.

3.2 Dynamics of minor constituents of the atmosphere in pulsed microwave discharges

The dynamics of minor constituents of the atmosphere were analyzed in paper [23] by numerical methods for an AIR created in the pulse-periodic regime close to the maintenance of an artificial radio mirror. The scheme used in the calculation included 166 reactions for 32 species in ground and excited states. So many processes are involved because the concentrations of different species are as a rule interrelated and, in the end, affect the dynamics of minor constituents of the atmosphere. The particle balance equation includes the natural sources of particles, which allowed a correct description of the unperturbed natural state and the process of relaxation to it. The electric field inhomogeneity, neutral gas heating, and plasma entrainment from the AIR were disregarded for the sake of simplicity. The calculation was performed for weak breakdown pulses with an electric field amplitude $E/E_{cr} = 3$, a pulse duration of 6 ns, and a pulse repetition period of 33 μs. Under such conditions, the electron concentration increased from pulse to pulse and fell slightly in the interval between them. The results of calculations are presented in Fig. 7. The figure shows that notable changes in the concentration of minor constituents do not occur immediately after the first breakdown pulse, but do occur after 10^2 pulses, when the electron concentration in the AIR becomes appreciable. At the end of the pulse series (marked in the figure by the vertical straight line corresponding to a sequence of 10^3 pulses), the ozone concentration exceeds the initial value by nearly an order of magnitude.

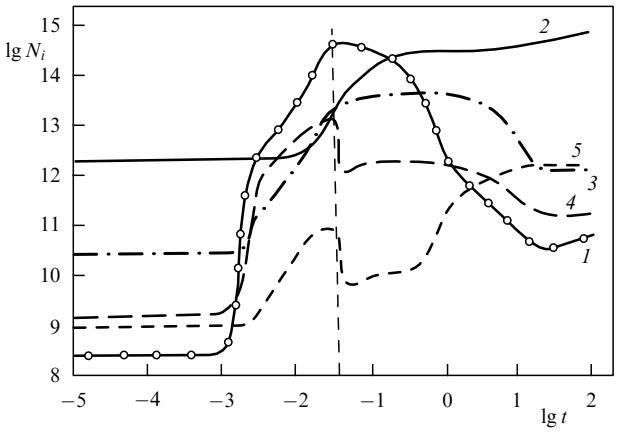

Figure 7. Variation of concentration of minor neutral and excited species during breakdown and relaxation at an altitude of 35 km: *1* — O, *2* — O_3, *3* — $O_2(^1\Delta_g)$, *4* — NO, and *5* — NO_2. The vertical dashed line marks the instant of action termination. The concentration N_i is given in units cm^{-3}, and the running time t in seconds.

The calculations showed that by the end of a train of 10^3 breakdown pulses the medium is strongly disturbed. The concentrations of various minor species (including nitric oxides) exceed their equilibrium values by several orders of magnitude. Such significant disturbances of the concentration of minor species upon a periodic breakdown mean that the relaxation process must proceed in a rather complicated way. The calculations also imply that for predominant ozone generation the conditions of AIR creation should differ essentially from those of radio mirror maintenance.

Indeed, as pointed out in Section 3.1, the process of ozone production in microwave fields consists of two stages. At first, oxygen molecules dissociate under the action of energetic electrons during each microwave pulse [reactions (11) – (13)]. Then, the resulting atomic oxygen becomes an ozone source in triple collisions [reaction (21)]. The characteristic time of atomic oxygen conversion into ozone determines the repetition period for a microwave pulse or a group of ionizing pulses, i.e. the modulation period (in seconds) which, with allowance for the numerical value of the rate constant of reaction (21), has the form

$$T_n = \frac{1.6 \times 10^{33}}{N_m[O_2]} \left(\frac{T}{300}\right)^2, \qquad (24)$$

where $[O_2]$ and N_m are the concentrations of oxygen and air molecules (in cm^{-3}) at the corresponding altitude. The characteristic T_n values for altitudes of 20 – 30 km are presented in Table 3.

We shall highlight some other important circumstances. First, for substantially smaller pulse repetition periods, atomic oxygen which provokes ozone decomposition in reaction (23) is accumulated in the AIR. To avoid this effect, the AIR location should be changed when the pulse repetition rate is high. Second, the repetition period (24) is nearly three orders of magnitude larger than the ionization relaxation time. Finally, for the creation of an atmospheric ozonizer, the choice of regimes in which nitric oxides, which lead to efficient ozone decomposition in catalytic reactions, are not accumulated is exceedingly important.

Thus, the theory points out that depending on the chosen regime of pulsed discharge in the AIR various impurity components may be produced: O, $O_2(^1\Delta_g)$, NO, NO_2, O_3. All of them are of interest for further investigation of the dynamics of minor constituents in real atmospheric experiments. The results of laboratory experiments simulating the plasma-chemical processes in an AIR created by nanosecond wave beams play, of course, an important role for finding the optimum ozone generation regime.

3.3 Laboratory studies of ozone and nitric oxide generation in microwave discharges in the air

The plasma-chemical processes in an AIR were simulated in a series of laboratory experiments [36 – 42] using various microwave radiation sources. In the first run of experiments, a relativistic carcinotron with an 8-mm wavelength range, pulse power $P = 10 – 25$ MW, pulse duration $\tau \approx 5$ ns, and pulse repetition rate $F = 1 – 10$ Hz was exploited. The second run was performed using a magnetron with a 3-cm wavelength range, pulse power $P_1 = 50$ kW, pulse duration $\tau_1 = 500$ ns, and pulse repetition rate $F = 10 – 1000$ Hz. To investigate the ozone synthesis during the course of shorter pulses, a microwave pulse compressor built around a superdimensional waveguide resonator was employed [41]. The device provided microwave pulses with a duration $\tau_2 = 6$ ns and power $P_2 = 800$ kW.

A schematic drawing of one of the experimental setups is presented in Fig. 8. The radiation from a microwave oscillator in the form of a Gaussian wave beam was directed onto a spherical metallic mirror with a diameter of 24 cm and a radius of curvature $R = 30$ cm. The mirror

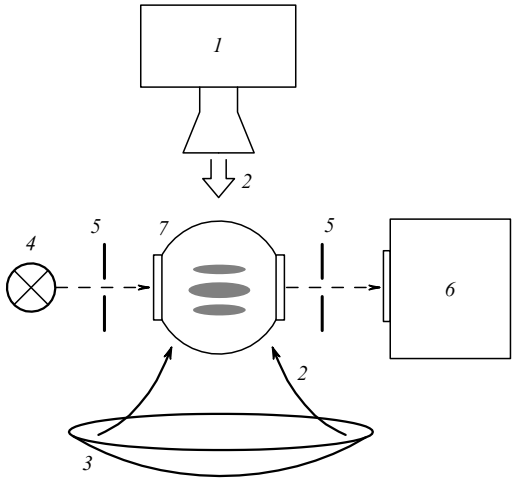

Figure 8. Schematic of the experimental setup: *1* — oscillator, *2* — microwave radiation, *3* — spherical mirror, *4* — hydrogen lamp, *5* — diaphragms, *6* — multichannel spectrum analyzer OVA-284, *7* — flask cooled by liquid nitrogen.

formed a wave beam which was focused into the center of a spherical quartz flask ~ 900 cm^3 in volume. The flask walls could be cooled by liquid nitrogen. The gaseous temperature was set in equal to the wall temperature and was varied within the range $T = 200-300$ K. The discharge was ignited at the mirror focus and constituted a set of plasmoids located at the antinodes of a standing wave formed by an incident electromagnetic wave and a wave reflected from the mirror.

The field strength E at the focus was determined by the air breakdown time τ_{br} through the relationship $\nu_i(E_{eff}/p) = \ln(N_{em}/N_{e0})/\tau_{br}$, where $\nu_i(E_{eff}/p)$ is the ionization frequency depending on the effective electric field E_{eff}, while N_{em} and N_{e0} are the final and initial electron concentrations. The electric field strength thus measured made up $E = 20-25$ kV cm^{-1}.

The experiments were performed in dry air at pressures $p = 10-90$ Torr. The pressure and temperature corresponded to the atmospheric conditions at altitudes $H = 15-30$ km. The remoteness of the discharge from the flask walls provided for the occurrence of chemical reactions in the volume inasmuch as the time of molecular diffusion towards the wall under the studied pressures substantially exceeded the characteristic time of the main chemical reactions responsible for the ozone synthesis. We shall also note that for a given arrangement of the experiment a regime of reaction product accumulation was realized and the conditions were simulated when during a pulse train the gas particles have insufficient time to leave the region occupied by the discharge.

The concentrations of ozone O_3 and nitrogen dioxide NO_2 molecules were measured by the absorbed UV radiant energy of a hydrogen lamp for the wavelengths $\lambda \approx 260$ and 360 nm, respectively, as given by the relation

$$I(\lambda) = I_o(\lambda)\exp(-\sigma_a N_a L)\,, \qquad (25)$$

where $I(\lambda)$ and $I_o(\lambda)$ are the intensities of transmitted and incident diagnostic radiations at a wavelength λ, L is the optical path, σ_a is the absorption cross section, and N_a is the concentration of the absorbing component. The absorption cross sections compiled in Refs [43, 44] were employed in processing the results.

A multichannel optical analyzer (OVA-284) served as a radiation detector. The OVA-284 spectrum analyzer was a spectral ruler with a resolution of 0.05 nm, interfaced with a computer. The data processing followed by their output to the display were done during the experiment. The time dynamics of the absorption spectrum were measured in a narrow spectral range of about 2 nm near the fixed wavelength. The number of chosen spectral ranges in which measurements were simultaneously taken could change from one to nine. The absorption spectrum was integrated over each spectral interval and was averaged over a time period of ~ 200 ms. The intensity fluctuations of the diagnostic radiation were controlled in the spectral region where the radiation was not absorbed by the plasma-chemical reaction products and were automatically taken into account in processing the results of measurements. The above-described data processing procedure substantially heightened the accuracy of measurements and made it possible to detect variations $\Delta I/I_o \sim 10^{-3}-10^{-4}$ in the intensity of light transmitted through the discharge region. The experimental errors were $\Delta[O_3] \approx 10^{12}$ cm^{-3} and $\Delta[NO_2] \approx 2 \times 10^{13}$ cm^{-3}, respectively.

The first series of experiments (at $T = 300$ K) revealed the following regularities of ozone production in the air. The ozone concentration linearly increases (Fig. 9) during the first pulses, reaches its maximum, and then falls off gradually to a low level. As the gas pressure is heightened, the O_3 concentration at the maximum increases, and the fall begins later. The NO_2 concentration exceeds the detection threshold at the instant when the ozone concentration passes through the maximum. Then the NO_2 concentration increases with decreasing O_3, reaches its maximum, and falls to a certain level.

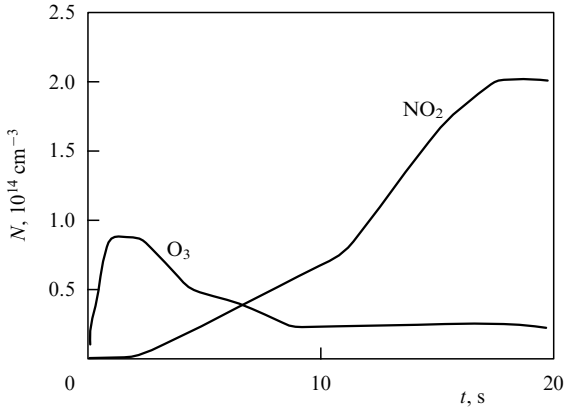

Figure 9. Time dependence of ozone and nitrogen dioxide concentrations at $T = 300$ K, $p = 75$ Torr, and $F = 3$ Hz.

When a small pulse train ($N = 3-30$ pulses) is exploited, the ozone decomposes after the end of a pulse sequence, and the larger the number of pulses in the train, the faster the ozone decomposition. After the decomposition, the ozone concentration stabilizes at a certain level. In a discharge in oxygen, no fall of O_3 concentration was observed.

Such dynamics of ozone content variation can be explained [39] by the formation and accumulation of stable ozone-decomposing chemical products in the vacuum chamber. The analysis of the characteristic time of O_3 decay

pointed to the reaction

$$NO + O_3 \rightarrow NO_2 + O_2\,,$$

$$k_3 = 4.3 \times 10^{-12} \exp\left(-\frac{1560}{T}\right) \text{ cm}^3\,\text{s}^{-1}\,, \qquad (26)$$

as the main cause of ozone decomposition. Such a reaction is responsible for the accumulation of nitrogen dioxide which, when concentrated highly enough, withdraws the atomic oxygen from the ozone generation process in the reaction [44]

$$NO_2 + O \rightarrow NO + O_2\,,$$

$$k_4 = 6.5 \times 10^{-12} \exp\left(-\frac{120}{T}\right) \text{ cm}^3\,\text{s}^{-1}\,. \qquad (27)$$

From reactions (21) and (27) one can find the value of the threshold NO_2 concentration with which the process (27) becomes determining for the loss of the oxygen atoms (at $T = 300$ K):

$$[NO_2^*] \geqslant [O_2][M]\frac{k_1}{k_4} \simeq 1.5 \times 10^{10} p^2\,. \qquad (28)$$

Here p is the pressure in torrs. When the nitrogen dioxide concentration reaches this $[NO_2^*]$ value, the ozone generation stops, process (26) leads to a decrease of the already reached O_3 concentration (see Fig. 9), and the number of decomposed NO_2 molecules is close to the number of oxygen atoms produced in one pulse. From Eqn (28) it also follows that the NO_2 concentration limiting the ozone content growth increases substantially with heightening air pressure. The NO_2 concentrations observed in the experiment before the fall of O_3 agree sufficiently well with the estimate (28). Thus, the measurements showed that at $p = 90$ Torr and $T = 300$ K approximately 5×10^{13} cm^{-3} of nitrogen dioxide is produced in a train of 10^2 pulses.

Initially NO can appear in various reactions, the most significant of which for low energy additions to the system is the reaction proceeding with the participation of nitrogen atoms [44]:

$$N + O_2 \rightarrow NO + O\,,$$

$$k_5 = 4.4 \times 10^{-12} \exp\left(-\frac{3220}{T}\right) \text{ cm}^3\,\text{s}^{-1}\,. \qquad (29)$$

However, on account of the high rate the reverse reaction [45]

$$NO + N \rightarrow N_2 + O\,, \qquad k_6 = 1.05 \times 10^{-12} T^{0.5} \text{ cm}^3\,\text{s}^{-1} \qquad (30)$$

restricts the nitric oxide formation. When the NO production is mainly determined by reaction (29), the steady-state NO concentration under a prolonged exposure to microwave radiation can be estimated from reactions (29) and (30):

$$[NO] \approx [O_2]\,\frac{k_5}{k_6} \approx \frac{10^{17}}{T^{0.5}} p \exp\left(-\frac{3220}{T}\right). \qquad (31)$$

From Eqn (31) it follows that the NO concentration cannot exceed the value of $[NO] \sim 4 \times 10^9 p$ cm^{-3} at $T = 300$ K. As the energy addition to the system increases, other channels of NO formation occur, for example, reactions with the participation of vibrationally excited N_2^*:

$$N_2^* + O \rightarrow NO + N\,, \qquad k_7 = 6.5 \times 10^{-12} \text{ cm}^3\,\text{s}^{-1} \qquad (32)$$

and metastable molecules through a reaction (17), which entail an increase of the nitric oxide concentration.

Measurements of the nitrogen vibrational temperature by the relative population of vibrational levels $v = 0-3$ of the electronic state $C^3\Pi_u$ (according to the method set forth in Ref. [46]) yielded the value of $T_v \approx 0.25$ eV. Such a vibrational temperature is threshold for reaction (32) [44], and the contribution of this reaction under our conditions may therefore be rather significant. We shall also note that according to Refs [45, 47] the rate constant of the reaction (32) for $T \leqslant 1000$ K weakly depends on the gaseous temperature.

Thus, the above-discussed laboratory studies point to the possibility of an appreciable gain of both ozone and nitric oxides in pulsed discharges in air. Obtaining the maximum possible ozone concentration and the minimum amount of nitric oxides in an ionized region at room temperature ($T \sim 300$ K) of air is only possible for a short-lived maintenance of the discharge, i.e. for a small number of microwave pulses in the train. The duration of discharge maintenance depends on the pulse repetition frequency and the pulse energy. In this case nitric oxides are not accumulated up to concentrations restricting ozone production.

It is exceedingly important that most of the above-mentioned reactions strongly depend on the gas temperature T. Therefore, in the real stratosphere at a low temperature $T = 200-220$ K the competition between the main processes of O_3 production may change radically. The dynamics of O_3 content variation at low gas temperatures were investigated to predict the effect of a microwave discharge on the stratosphere.

Figure 10 presents the time dependence of O_3 concentration for $p = 30$ Torr with lowering gas temperature. The NO_2 gain in these experiments did not overstep the measuring method sensitivity of $\sim 10^{13}$ cm^{-3}. The figure shows that on lowering the temperature to 215 K, the ozone concentration increased at all pressures by more than an order of magnitude, while an $[O_3]$ fall was not observed even after a long-term exposure. Figure 11 presents the time dependence of ozone concentration for a fixed neutral particle concentration $N_m = 2 \times 10^{18}$ cm^{-3} (which corresponds to the height $H = 20$ km) for various gas temperatures. The maximum

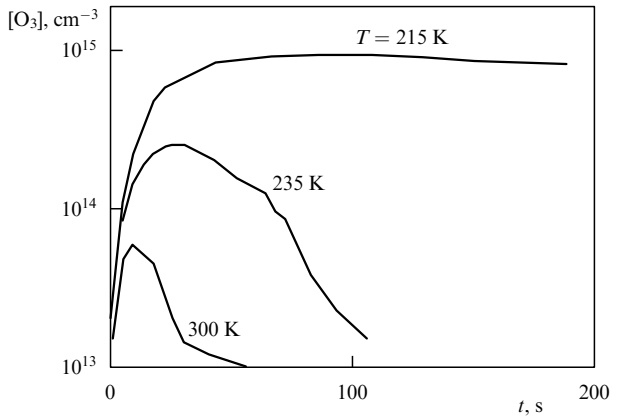

Figure 10. Time dependence of the ozone concentration at different air temperatures ($p = 30$ Torr and $F = 3$ Hz).

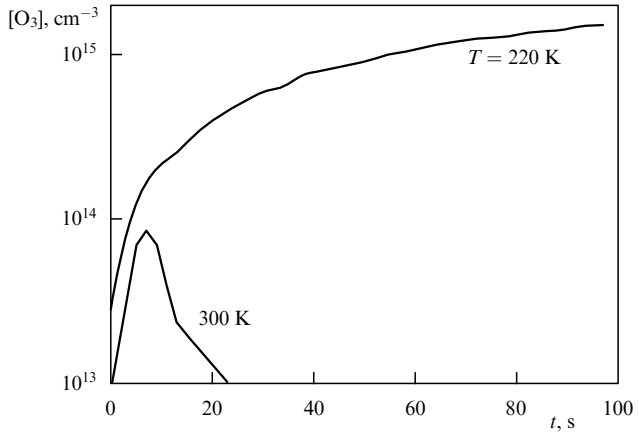

Figure 11. Time dependence of the ozone concentration for a given neutral particle concentration $N_m = 2 \times 10^{18}$ cm^{-3}, $F = 3$ Hz and various air temperatures.

ozone concentration at investigated pressures increased proportionally to the air pressure.

The analysis shows that lowering the gas temperature leads to an increase of the ozone production rate in reaction (21) and simultaneously sharply lowers the nitric oxide production efficiency in reaction (29). According to the estimates, the concentration of ozone produced in a single discharge pulse at a pressure $p = 90$ Torr made up $(2-3) \times 10^{12}$ cm^{-3}, whereas the nitrogen dioxide concentration did not exceed 10^{10} cm^{-3}.

Thus, in creation of a microwave discharge in the atmosphere, conditions can be reached when the nitrogen dioxide concentration does not exceed the natural level [1], while the O_3 concentration corresponds or even appreciably exceeds the concentration at the maximum of the ozone layer.

3.4 The energy cost of ozone molecule production

An important characteristic necessary for outlining the prospects of the advent of an atmospheric ozonizer is its energy efficiency. Experimental studies have shown that the ozone production efficiency substantially depends on the discharge-generating electrodynamic system. In particular, for systems of standing wave type or crossed wave beams the efficiency appears to be higher than in the creation of a discharge with the aid of a convergent cylindrical *TE* wave [48].

In experiments, the discharge was initiated in two essentially different electrodynamic systems demonstrated in Fig. 12a, b. In the first case (Fig. 12a), the microwave radiation was focused by a deep mirror with the shape of a parabolic cylinder, so that the electromagnetic field in the breakdown region was close to a standing cylindrical *TE* wave (the electric field vector **E** was aligned with the focal axis of the mirror). The discharge was cylinder-shaped and had a diameter of several millimeters, and a length of about 30 cm. In the second case (Fig. 12b), an almost plane standing electromagnetic wave was formed by a spherical mirror in its focal region, and the discharge constituted a set of plasmoids having a diameter of nearly 3 cm and localized in the standing wave antinodes. In view of the large extent of the discharge, the cylindrical geometry facilitated ozone concentration measurements, while the planar geometry rather corresponded to the regimes of a discharge creation

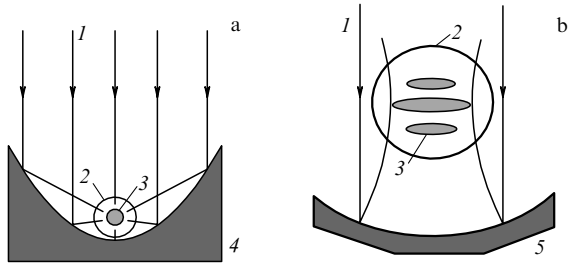

Figure 12. Schematic of discharge creation using a parabolic cylinder (a) and a spherical mirror (b): *1* — microwave radiation, *2* — quartz flask, *3* — discharge plasma, *4* — a parabolic cylinder as mirror, and *5* — spherical mirror.

in the upper Earth atmosphere by means of crossed wave beams.

The energy cost of producing one ozone molecule was measured at the stage of the linear growth of ozone concentration (when the number density of its decomposers is small) and was determined as the ratio of the energy emitted by the microwave oscillator to the total number of the O_3 molecules produced:

$$\eta = \frac{P\tau n_p}{[O_3]V}, \tag{33}$$

where n_p is the number of microwave pulses, $[O_3]$ is the ozone concentration after n_p pulses, and V is the flask volume.

Notice that calculations using formula (33) yield an overestimated energy cost because they disregard the microwave energy losses occurring mainly for two reasons. First, part of the energy was reflected by the flask walls. Second, owing to the nonuniform spatial field distribution in the beam, the gas breakdown appeared in its central region, while on the periphery the electromagnetic energy was not absorbed by the plasma.

The dependence of the energy cost on the air density for the two cases described above is given in Fig. 13. The scatter of the experimental points is due to the instability of the

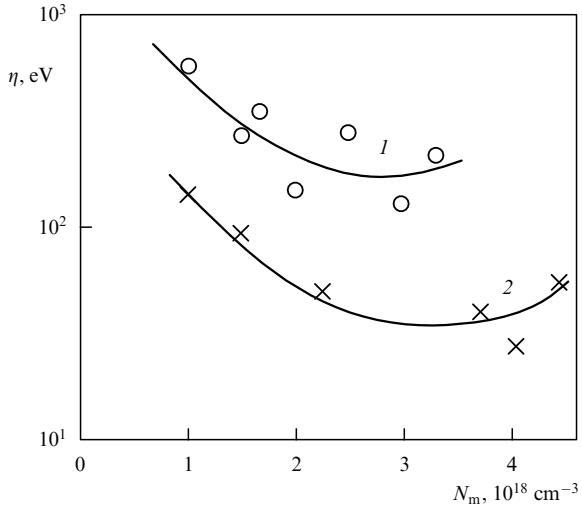

Figure 13. Experimental dependence of the energy cost of producing one ozone molecule on the air density in fields of electromagnetic waves close to cylindrical (*1*) and planar (*2*) geometry.

microwave-oscillator pulse power on which, as shown below, the energy cost depends rather strongly. Figure 13 demonstrates that the energy cost of ozone production decreases with increasing air density, the energy cost in quasi-planar geometry being much lower than in cylindrical geometry.

The results of the model experiments performed suggest that an efficient way to obtain ozone in the atmosphere has been found. A nanosecond microwave discharge can efficiently generate ozone. In laboratory experiments, rather low expenditures of energy for the production of one ozone molecule ($\eta = 15-20$ eV per molecule) have been demonstrated. Such an energy cost corresponds to the production of 100 g of ozone per 1 kW · h of consumed electric energy.

In nanosecond discharges, the main part of the microwave energy absorbed in the plasma is expended in doing ionization, dissociation, and excitation of electron levels of O_2 and N_2 molecules. The formation of oxygen atoms then converted to ozone mainly proceeds through the dissociation of O_2 molecules by electron impact (11) and in O_2 collisions with metastable N_2 molecules [reaction (12)]. The rate constants of processes (11) and (12) are specified by the energy distribution function of electrons and depend on the electric field strength in the plasma. The values of the oxygen dissociation rate constant k_d in process (11) are rather well known for a constant electric field [49, 50]. Making use of these data, we shall estimate the expenditure of energy for the production of one ozone molecule in a microwave discharge. Suppose that all the atomic oxygen produced in the dissociation process (11) enters into the ozone synthesis reaction (21). The estimate will be based on the equation describing the production of oxygen atoms per pulse, viz.

$$\frac{d[O]}{dt} = 2k_d[O_2]N_e\,. \tag{34}$$

The concentration of ozone produced in a single microwave pulse can be estimated from formula (34) as

$$[O_3] = [O] = 2k_d\,\frac{E_{eff}}{N_m}\,[O_2]N_e\tau\,. \tag{35}$$

The expenditure of energy for the production of one ozone molecule is obtained from the ratio of the microwave energy absorbed in the plasma to the ozone concentration [51]:

$$\eta = \frac{\sigma E^2\tau}{2k_d[O_2]N_e\tau} = \alpha\,\frac{e^2}{m}\left(\frac{\nu_c}{N_m}\right)^{-1}\frac{(E_{eff}/N_m)^2}{k_d}\,, \tag{36}$$

where $\sigma = e^2N_e\nu_c/m(\nu_c^2+\omega^2)$ is the plasma conductivity, and $\alpha = 1/2$ and $5/2$ for oxygen and air, respectively. From Eqn (36) it is easy to specify the optimum conditions when for a given microwave pulse energy the number of O atoms occurring in the ionized region is maximum. The quantity $(E_{eff}/N_m)^2/k_d$ has its minimum for the reduced effective electric field E_{eff}/N_m described by the expression

$$\frac{E_{eff}}{N_m} = \frac{2k_d}{dk_d/d(E_{eff}/N_m)}\,. \tag{37}$$

Under the optimum condition (37), the oxygen molecule dissociation requires the maximum possible fraction of the microwave pulse energy. Notice that these conditions are similar to the optimum conditions of maximum expenditure of energy for the ionization (7) in a nanosecond microwave discharge.

Figure 14 gives the dependence of η, calculated using formula (36), on the reduced electric field strength E_{eff}/N_m in oxygen (curve *1*). The graph shows that under the optimum conditions the magnitude of the field is either smaller than or of the order of the threshold value necessary for a microwave breakdown of oxygen. It should be emphasized that the low energy cost of ozone molecule production for a discharge in oxygen, $\eta \sim 3$ eV per molecule, was obtained in the experiment [52], in which the discharge was created in a cavity resonator. Plasma formation led to a shift of the resonance frequency of the cavity and thus to a decrease of the electric field strength and maintenance of a pulse-periodic discharge in the prebreakdown field.

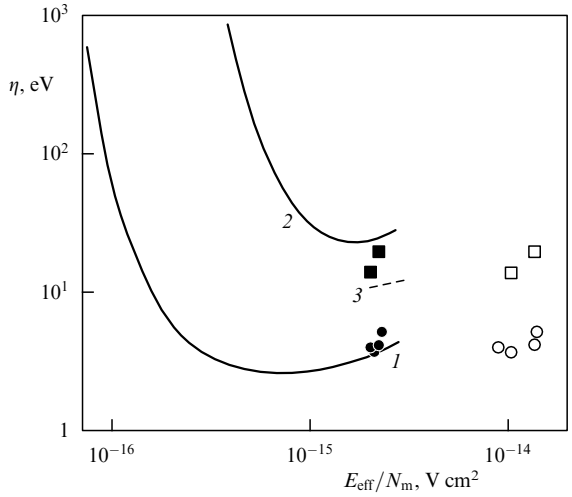

Figure 14. Dependence of the expenditure of energy for the formation of one ozone molecule on the reduced electric field in a plasma. Calculation: *1* — oxygen, *2*, *3* — air; experiment ($\tau = 6$ ns): ○, ● — oxygen, □, ■ — air. The intensity of the effective field E_{eff} was determined by the prebreakdown electric field strength (○, □) or was calculated in the plasma (●, ■).

In the air, as has already been noticed, two O atom production channels are possible, namely, direct O_2 molecule dissociation and an indirect channel through reactions (12) and (14). With allowance for direct dissociation alone, one can calculate the dependence of the expenditure of energy for O_3 production on the reduced electric field. In Fig. 14 (curve *2*), the dependence $\eta(E_{eff}/N_m)$ was calculated using formula (36) for a microwave discharge in the air using the rate constants of the direct O_2 dissociation in the air, borrowed from paper [53]:

$$k_d = 10^{-[A+B/(E_{eff}/N_m)]}\,, \tag{38}$$

where A and B are the numerical coefficients (see Ref. [53]). It was taken into account that the oxygen molecule dissociation in reaction (11) proceeds from three electronic levels, and therefore in the calculation of η the resultant constant k_d was employed.

Figure 14 also presents the experimental data on a discharge formed by a quasi-plane standing wave in oxygen and air [41]. The magnitude of the effective field E_{eff} was determined by the electric field strength in the discharge region prior to the breakdown onset (first version) and was calculated in plasma (second version) for a discharge in the field of a plane standing wave [48]. When evaluating E_{eff} we assumed the electron collision frequency (s^{-1}) to be equal to

$\nu_c = 3.7 \times 10^9 p$ and $5.3 \times 10^9 p$ in oxygen and air, respectively [54].

As we can see from the figure, the experimental η values in the air are smaller than those estimated by formula (36). This points to the fact that the O_2 molecule dissociation channel connected with the excitation of the electronic levels in N_2 molecules plays an important role in the plasma of a nanosecond microwave discharge in the air. It is known, for instance, that in ozonizers operating on the basis of barrier discharge, from 50 to 90% of O_2 dissociation events in the air are realized through the indirect channel [55]. The calculations of the O_2 molecule dissociation rate constant with allowance for the processes (12), (14), carried out in Ref. [56] for a microwave discharge in the air, also testify in favor of the indirect channel as the main O_2 dissociation channel. Figure 14 (curve *3*) presents the calculated results of the expenditure of energy for ozone production involving the contribution of the electron-excited states of nitrogen molecules, calculated in paper [56]. We can see that they are in better agreement with observations.

Thus, the optimum conditions for oxygen dissociation exist in the air too, but as distinct from a discharge in oxygen [51], their determination is a more complicated task. Note that the above estimates referred to finding the optimum conditions for the production of oxygen atoms. For a discharge initiated by single nanosecond microwave pulses (or a small train of microwave pulses), these estimates are valid for ozone as well because ozone-decomposing particles do not have time to accumulate and the gas is not heated substantially. The energy cost of ozone production in this process is determined by the discharge electrodynamics and depends on how fast the optimum conditions of oxygen molecule dissociation are reached and how long they are maintained in the discharge plasma.

The conditions of efficient ozone generation (without gas heating and accumulation of ozone-decomposing particles in the discharge region) can seemingly be reached not only in a nanosecond microwave discharge [52]. A low energy cost of ozone molecule production was obtained in an experiment where the discharge was created in a microwave cavity resonator (Fig. 15). A cylindrical cavity 50 cm in length and 7 cm in diameter was excited on the TE_{11p} mode. The experiments were performed under the following conditions: the wavelength was 5 cm, the pulse duration — 2.5 μs, the oscillator pulse power — 0.1–9 kW, the pulse repetition rate — 330 Hz, and the air pressure $p = 1-30$ Torr. The loaded Q factor of the cavity resonator was equal to ~ 300. The experiments were carried out with air circulation through the cavity at a low rate of 0.5 l min^{-1}. The cavity resonator walls could be cooled by liquid nitrogen vapors. The air temperature was set equal to the wall temperature and can be varied within the range $T = 250-300$ K.

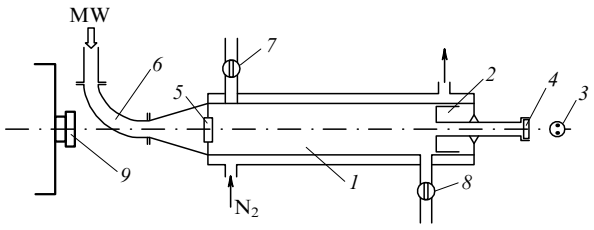

Figure 15. Schematic of the experimental setup: *1* — waveguide resonator on the TE_{11p} mode with double walls for cooling by liquid nitrogen vapor, *2* — plunger, *3* — mercury lamp, *4* and *5* — input and output quartz windows, *6* — waveguide channel, *7* and *8* — inlet and escape valves for air circulation, *9* — monochromator.

This experiment showed evidence of a low expenditure of energy $\eta = 5$ eV for the production of one ozone molecule (Fig. 16). This is evidently because the mean electron concentration in the cavity resonator was much smaller than the critical one for microwave radiation frequency and made up $\sim 10^9$ cm^{-3}.

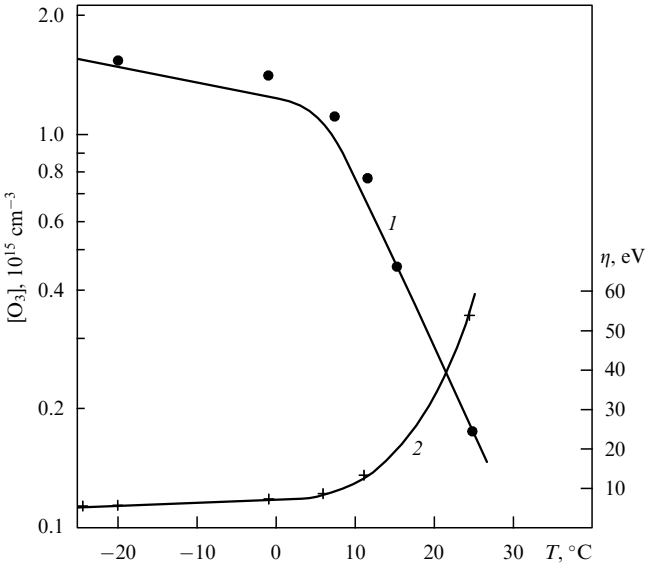

Figure 16. Dependence of the mean ozone molecule concentration (*1*) and of the energy cost of ozone molecule production (*2*) on the resonator wall temperature.

The low electron concentration N_e was maintained by a strong feedback between the resonator and the microwave oscillator. In turn, the gas was not heated noticeably because of the low N_e and neither were ozone-decomposing particles accumulated owing to the gas circulation through the resonator. This experiment testifies to the possibility of further lowering the energy cost of ozone molecule production, which has been obtained in nanosecond microwave discharges.

4. Ozone generation in the stratosphere via an AIR

Laboratory experiments and theoretical estimates have shown that in nanosecond microwave discharges at stratospheric gas pressures and temperatures, ozone can be efficiently generated with an expenditure of energy (100 g of ozone per 1 kW·h of electric energy) corresponding to the best contemporary ozonizers. However, in reality atmospheric processes are determined by a multitude of physicochemical processes hardly reproducible in laboratory conditions. The following questions arise: What will be the fate of ozone and other impurities additionally generated in the atmosphere? What are the best altitudes for ozone generation? What changes in the ozone layer distribution may an artificial atmospheric ozonizer induce? Answers to these and other questions can be found through numerical simulations.

4.1 Ozone generation and decomposition under natural conditions

The generation and decomposition of ozone in the atmosphere are largely of photochemical origin. The Earth's atmosphere absorbs solar radiation well in the UV region. Three UV spectral regions are typically distinguished, namely, the near ultraviolet region from 320 to 400 nm (UV-A), the middle ultraviolet from 290 to 320 nm (UV-B), and the far ultraviolet from 200 to 290 nm (UV-C). The maximum response of biological objects (per unit radiation energy), which frequently exceeds the changes induced by harder X-ray radiation, falls precisely within these wavelength ranges.

Radiation with a wavelength shorter than 200 nm is very efficiently absorbed by oxygen molecules and disappears almost completely at altitudes of 20 – 25 km. In this spectral region, absorption is accompanied by the decomposition (photodissociation) of the absorbing molecules into atoms:

$$O_2 + h\nu \rightarrow O + O\,, \tag{39}$$

$$N_2 + h\nu \rightarrow N + N\,. \tag{40}$$

Here $h\nu$ is a light quantum (photon) with an energy exceeding the atomic binding energy in a molecule (for oxygen, this corresponds to radiation with a wavelength $\lambda \leqslant 240$ nm).

As distinct from the UV-C region, UV radiation in the B region remains practically unabsorbed by the main atmospheric gases. But the chemical composition of the atmosphere changes under the action of a harder radiation. Photodissociation of atmospheric molecules induces the production of free radicals and atoms, for example, oxygen O and nitrogen N atoms, nitric oxide NO and hydroxide OH molecules. The distinctive feature of these particles is their high chemical activity allowing them to enter into reactions even with chemically stable compounds. For instance, the oxygen atoms appeared due to molecular photodissociation promote production of ozone molecules O_3 in reaction (21). It is precisely reactions (39), (21) – (23), which were first examined by the well-known English geophysicist S Chapman in 1930, that largely determine the equilibrium ozone concentration set in the atmosphere [1]. An important feature of the ozone molecule is that it absorbs UV radiation rather efficiently in precisely the B spectral region. Ozone photodissociation under the action of UV radiation in the reaction

$$O_3 + h\nu \rightarrow O_2 + O \tag{41}$$

at high altitudes (in the region of a low atmospheric density) and the absence of oxygen dissociation at low altitudes, where hard UV radiation does not penetrate, lead to the formation of the ozone layer in the atmosphere. The ozone layer is quite thin. If we imagine that this ozone were completely accumulated on the Earth's surface, at a normal pressure it would cover the latter with a layer only 2 – 3-mm thick. Nevertheless, this particular layer serves as a 'wonderful shield' which protects the Earth from the destructive effect of solar radiation.

Investigations have shown that a significant role in the ozone layer formation and ozone decomposition in the atmosphere is played by the above-mentioned catalytic cycles. These cycles accelerate chemical reactions through a catalytic agent which repeatedly enters into intermediate reactions and is restored after the end products are produced. For the ozone decomposition process, the catalytic cycle can be described by the reactions

$$O_3 + X \rightarrow XO + O_2\,, \tag{42}$$

$$O + XO \rightarrow X + O_2\,. \tag{43}$$

Comparing the left- and right-hand sides of reactions (42) and (43), one can readily see that the cycle is responsible for the loss of the oxygen atom and the ozone molecule upon their direct interaction as in reaction (23). Different chemical compounds and elements, namely, nitric oxide NO, hydroxide OH molecules, and chlorine Cl atoms may serve as the catalyst X for the ozone. Accordingly, nitrogen, hydrogen, and chlorine catalytic cycles of ozone decomposition are distinguished. They induce a multifold (several orders of magnitude) increase of the rate of reaction (23) causing ozone loss.

It should be emphasized that in the atmosphere the majority of compounds that come out as such catalysts are of anthropogenic (resulting from human activities) origin. For example, nitric oxides and hydrogen radicals are contained in the gas exhausts from numerous factories, thermoelectric power stations and various transport facilities, and the sources of chlorine are Freons (carbon fluorides and chlorides) widely employed in refrigerators, fire extinguishers, and aerosol flasks. Having low chemical activity, Freons are capable of reaching ozone layer altitudes where they dissociate by action of UV radiation, and the chlorine atoms liberated in such a photodissociation enter into catalytic reactions with ozone [57]. The lifetime of Freons in the atmosphere is tens of years [58]. In view of long-standing occurrence of minor impurities in the atmosphere and poor control over their penetration into the atmosphere, a long-term forecast of the state of the ozone layer is difficult. However, as shown above, both additional ozone generation and the generation of nitric oxides — other minor constituents that play an important role in catalytic processes — are possible in an AIR created in the atmosphere. A change in the AIR operating conditions permits efficient variation of the generation regimes. So, with allowance for this circumstance, the use of an AIR may provide efficient sensing of the ozone layer state via controllable generation of additional ozone and insignificant amounts of some minor constituents. Measuring their concentrations in the AIR and observing the establishment of equilibrium, one can determine the composition of the AIR atmosphere and gain information on the effect of minor constituents on the ozone layer.

4.2 Optimum position for the source of additional ozone

To evaluate the optimum altitude for a source of additional ozone, we shall first of all examine the simplest model, the so-called Chapman model [1] which considers only oxygen air components interacting between themselves and with solar UV radiation. In this case, the family of odd oxygen O_x is naturally singled out, which includes ozone and excited oxygen atoms: $O_x = O_3 + O(^3P) + O(^1D)$. The concept of the family is convenient here because the fastest reactions lead only to a member redistribution inside the family. That is why dynamic equilibrium among the components O_3, $O(^3P)$, and $O(^1D)$ is established in the family. When the ozone concentration appreciably exceeds the atomic oxygen concentration, we have $O_x \approx O_3$. This means that the actual ozone lifetime may substantially exceed its photochemical lifetime. So, for instance, at an altitude of ~ 20 km the photochemical ozone

lifetime makes up $\tau_{O_3} \approx 1$ h, while the family lifetime is $\tau_{O_x} \approx 1$ year [59].

We shall be interested in the relaxation times τ_p of the initial ozone perturbation to equilibrium. Table 4 presents the relaxation times in days, calculated within the Chapman model for heights $H = 20$, 25, 30, and 35 km at different latitudes for three months (October, November, and December) [59]. The computations allowed for the dependence of UV radiation on the zenith angle of the Sun and exploited the CIRA-86 model for the air temperature and air component concentrations. The initial perturbation $\delta[O_3]$ of the ozone concentration was given by

$$\delta[O_3] = \alpha[O_3^{(o)}] \exp\left[-\frac{(z-H)^2}{\Delta H^2}\right], \qquad (44)$$

where $[O_3^{(o)}]$ is the equilibrium ozone concentration, ΔH the half-width of the artificial ozone layer (AOL), H the altitude of the layer center position, and α the relative perturbation which was varied within the limits $0.5 \leqslant \alpha \leqslant 2$. Table 4 presents the relaxation times τ_p corresponding to the value $\alpha = 1$. One can see a sharp decrease of the relaxation time τ_p with altitude. A much weaker effect on the relaxation times is produced by variations of the initial perturbation ($\alpha = 0.5$, $\alpha = 2$).

Table 4

H, km	Relaxation times of ozone perturbation τ_p, d					
	Latitude 40° S			Latitude 30° S		
	October	November	December	October	November	December
20	257	276	287	311	341	355
25	36	36	34	37	38	37
30	9	8	7	8	8	8
35	3	2	2	3	2	2

The above results suggest sufficiently low AOL altitudes as most advantageous because the layer lifetime increases rapidly with decreasing altitude. However, the expenditure of energy on layer maintenance at low altitudes grows sharply. It could therefore be expected that AOL creation is most reasonable at altitudes near the maximum of the natural ozone layer. This conclusion is confirmed by rigorous numerical calculations simulating the realistic conditions of the atmosphere [60]. Figure 17 demonstrates the vertical profiles of stationary ozone concentration variations due to the action of an additional ozone source placed within the two-kilometer-height layer with centers alternately at altitudes $H = 10$, 14, 16, 18, 20, and 22 km. The intensity of the ozone molecule source was assumed to be equal to $Q_{O_3} = 6.8 \times 10^5$ cm^{-3} s^{-1} without specification of the ozonizer operation principle. The maximum increment of the total ozone content was 11% when such an additional ozone source was positioned at an altitude of 18 km. The additional ozone production led now to a decrease of NO, NO_2, Cl, and HCl content in the atmosphere and to a certain increase of HNO_3, H_2O, and ClO concentrations, while the additional atmosphere heating did not exceed 3 K.

For comparison purposes we shall estimate the ozone generation intensity in an AIR. Let us use the above equation (34) describing the production of oxygen atoms during a microwave pulse. We assume the atomic oxygen appeared owing to O_2 molecule dissociation to be totally converted to

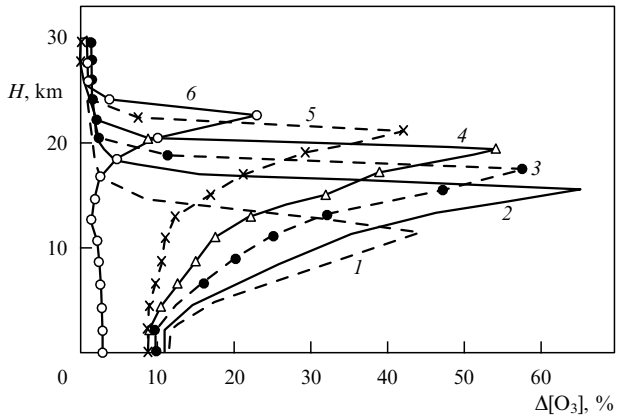

Figure 17. Vertical variation profiles of the stationary average global, average annual ozone concentration under the action of an additional ozone source with an intensity of 100 kt h^{-1} positioned at altitudes of 10 km (*1*), 14 km (*2*), 16 km (*3*), 18 km (*4*), 20 km (*5*), and 22 km (*6*) [60].

ozone. For the microwave pulse repetition period T_n, the number of ozone molecules produced per 1 cm^3 per 1 s in an AIR is equal to

$$\bar{Q}_{O_3} = \frac{\tau}{T_n} 2k_d \left(\frac{E}{E_{cr}}\right)[O_2]N_e\,. \qquad (45)$$

The reaction rate constant k_d for oxygen molecule dissociation by electron impact can be found from formula (38). When an AIR is created, for example, at an altitude $H = 20$ km under the optimum conditions (7) and with a pulse duration of $\tau = 50$ ns (for $\tau/T_n = 4 \times 10^{-5}$), the ozone source intensity makes up $\bar{Q}_{O_3} \approx 2 \times 10^{17}$ cm^{-3} s^{-1}. As the example illustrates, the AIR is an intensive ozone source, but ozone is generated in a small volume, where the initial electric field E_0 markedly exceeds the critical value E_{cr}. It should also be considered that in the actual atmosphere there exists another efficient channel of atomic oxygen production, namely, the reaction with electronically excited nitrogen molecules [reaction (12)]. Moreover, the breakdown pulse repetition period T_n can be shortened essentially if the AIR position undergoes changes. All this may lead to a notable increase of the ozone source strength.

Not only atomic oxygen, but also atomic nitrogen as well as electronically excited nitrogen and oxygen molecules are produced during each microwave pulse in an AIR. All these particles are chemically active. Their interaction with other air components induces changes in the concentration of various minor neutral components. Under the action of atmospheric wind and turbulent diffusion, the reaction products are taken out of the discharge and in the course of further interaction gradually fill a vast area. If, in the discharge, the ozone production is predominant, one can speak about the formation of an artificial ozone layer. The most important parameter characterizing the AOL is its relaxation time. This time determines, in particular, the layer dimensions and the expenditure of energy for its creation. In the framework of the Chapman model, the AOL relaxation time was discussed above. In realistic conditions of the atmosphere, the relaxation time is affected by the concentrations of other minor species, first of all nitric oxides. That is why it is important to choose such conditions for AOL creation under which ozone production is predomi-

nant, while nitric oxide concentrations remain at the background level.

4.3 Calculations of the energy cost of ozone production in an AIR

The energy cost of ozone production in an AIR created in the stratosphere by crossed wave beams was calculated in Ref. [48]. Note that an exact calculation of the discharge dynamics in crossed beams with a large aperture ($\sim 100\lambda$) is rather complicated even in the two-dimensional approximation and requires much computer time. For this reason we shall avail ourselves of the one-dimensional model which was used in the description of the discharge dynamics in crossed *TE* beams in Refs [20, 21, 61]. This model, although not completely describing the discharge space-time dynamics, still reveals the basic laws of its development.

In this model, the field distribution is governed by the equation

$$\frac{\mathrm{d}^2E}{\mathrm{d}x^2}+k^2\left[\sin^2\theta-\frac{N_\mathrm{e}}{N_\mathrm{cr}}\left(1+\mathrm{i}\,\frac{\nu_\mathrm{c}}{\omega}\right)\right]E=0\,, \tag{46}$$

where $k=\omega/c=2\pi/\lambda$ is the wave number, N_cr the critical electron concentration, 2θ the angle between the beam axes, and the x axis is perpendicular to the bisectrix of this angle and lies in the plane passing through the beam axes (see Fig. 2). Equation (46) was solved in Ref. [61] on the segment $-L\leqslant x\leqslant +L$, where L is the coordinate of an arbitrary point outside the AIR. For $x=\pm L$, the boundary conditions were specified, corresponding to the incidence of two counter-propagating waves on the discharge region.

It is readily seen that equation (46) is equivalent to the one-dimensional Helmholtz equation for the complex amplitude of the field E with a complex dielectric constant ϵ:

$$\frac{\mathrm{d}^2E}{\mathrm{d}z^2}+\varepsilon k^2E=0\,,\qquad \epsilon=1-\frac{N_\mathrm{e}}{N_\mathrm{cr}\sin^2\theta}\left(1+\mathrm{i}\,\frac{\nu_\mathrm{c}}{\omega}\right),$$
$$z=x\sin\theta\,. \tag{47}$$

Allowing for the symmetry of the initial problem about $x=0$ and assuming $E(x=0)=0$ (an even number of antinodes in an AIR), one can replace the solution on the segment $-L\leqslant x\leqslant +L$ by the solution in the domain $0\leqslant z\leqslant m\lambda$ with the following boundary conditions. At the point $z=0$, the total reflection condition

$$E\Big|_{z=0}=0 \tag{48}$$

is imposed. At the point $z=m\lambda$, the electric field is represented as the sum of an incident and a reflected waves:

$$E\Big|_{z=m\lambda}=\left[A\exp(\mathrm{i}kz)+G_\mathrm{ref}A\exp(-\mathrm{i}kz)\right]\Big|_{z=m\lambda}$$
$$=A(1+G_\mathrm{ref})\,, \tag{49}$$

$$\frac{\mathrm{d}E}{\mathrm{d}z}\bigg|_{z=m\lambda}=\mathrm{i}k\left[A\exp(\mathrm{i}kz)-G_\mathrm{ref}A\exp(-\mathrm{i}kz)\right]\Big|_{z=m\lambda}$$
$$=\mathrm{i}kA(1-G_\mathrm{ref})\,, \tag{50}$$

where A is the amplitude of the incident wave which was assumed to be given, and G_ref is a complex quantity determined by the sum of a transmitted wave incident from the left and the reflected wave propagating from the right. Thus, the simplified discharge dynamics in crossed *TE* beams can be described in the framework of the model (47) – (50).

We shall assume for definiteness that an AIR is created by two ground-based antennas located at a distance of 30 km from each other at altitudes $H=20$, 25, and 30 km (in the ozone layer) which correspond to the air number densities $N_\mathrm{m}=1.9\times10^{18}$, 7.7×10^{17}, and 3.6×10^{17} cm^{-3}. The calculations were performed for two wavelengths $\lambda=3$ cm and 8 mm. When microwave radiation is focused at these altitudes, the focal region of the beams reaches sizes in the range $(50-150)\lambda$. We shall choose a rather long ($\tau\gg L/c$) microwave pulse duration in order that the finite spatial length of the microwave pulse might be neglected.

Figure 18 presents the energy costs of the oxygen atom production as functions of the initial electric field E_0 in an AIR, calculated under these assumptions. The calculations show that for moderate fields the lowest energy cost (of about 30 – 40 eV) is reached for $\lambda=3$ cm at an altitude $H=25$ km and an initial field strength $E_0=4$ kV cm^{-1}, and for $\lambda=8$ mm — at an altitude $H=20$ km and initial field strength $E_0=8$ kV cm^{-1}. Such intensities of the electric field can be attained by focusing two electromagnetic wave beams from antennas nearly 100 m in diameter. The radiation power in each beam must be $P=9$ GW for $\lambda=3$ cm, and $P=2$ GW for $\lambda=8$ mm. As we can see, antenna complexes necessary for efficient oxygen dissociation through a microwave discharge in the atmosphere may well be created with the contemporary level of technology.

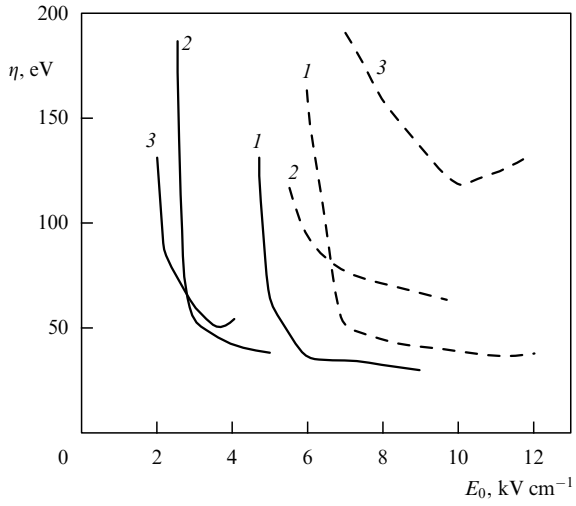

Figure 18. Energy cost of oxygen atom production in an AIR created at altitudes of 20 km (*1*), 25 km (*2*), and 30 km (*3*) as a function of the initial electric field strength. The microwave radiation had a wavelength of 3 cm (solid lines) and 8 mm (dashed lines) and a pulse duration $\tau=50$ ns.

Notice that the obtained intensities of the electric field E_0 are close to those necessary for efficient creation of an artificial radio mirror [19] where the largest fraction of the microwave pulse energy is expended on ionization (7): $E_0/E_\mathrm{cr}=5-7$ for a pulse duration $\tau_0=\ln(N_\mathrm{em}/N_\mathrm{e0})/\nu_\mathrm{i}(E_0)$, where E_cr is the critical field (1), ν_i is the electron ionization frequency (2), N_e0 and N_em are the initial and final electron concentrations. To produce the maximum amount of atomic oxygen, the microwave pulse duration should be several times greater than τ_0. Figure 19 gives the calculated dependence of the energy cost of oxygen atom production on the microwave

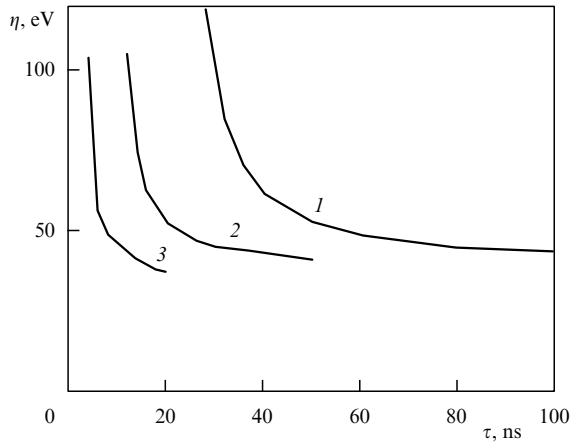

Figure 19. Energy cost of oxygen atom production versus the microwave pulse duration ($\lambda = 3$ cm) for different initial electric field strengths in the AIR (*1* — 3 kV cm^{-1}, *2* — 4 kV cm^{-1}, and *3* — 6 kV cm^{-1}) at an altitude $H = 25$ km ($N_m = 7.7 \times 10^{17}$ cm^{-3}).

pulse duration for different initial field intensities E_0 in the beam crossing region at an altitude $H = 25$ km. The calculations only involved the oxygen molecule dissociation, i.e. the first stage necessary for ozone generation. As a matter of fact, not all the oxygen atoms produced in a discharge go into ozone generation in process (21); some of them enter into reactions with nitric oxides both contained in the atmosphere and turned out in the discharge itself. However, at the low gaseous temperature typical of the ozone layer region, nitric oxides interact with a small portion of oxygen atoms [40]. The energy cost of ozone production will therefore be close to that of oxygen atom production.

4.4 Relationship between [O_3] and [NO_x] in an ionized region

The question of the presence of side effects is very important for the initiation of a microwave discharge in the atmosphere. In the first place it is necessary to estimate the production of nitric oxides. The [O_3]-to-[NO_x] ratio depends essentially on the energy addition to the discharge plasma [62]. Figure 20 illustrates the results of calculations of the ratio $[O_3]/([NO] + [NO_2])$ depending on the specific energy addition to the discharge for the initial electric field E_0 in which the energy cost of ozone generation is minimum (see Fig. 18). In the calculations, the energy addition to the system was changed by varying the microwave pulse duration and leaving the initial electric field unchanged. The computations were based on the model described in Section 4.3 for microwave radiation of three-centimeter wavelength range, directed to the stratosphere by two ground-based antennas with a diameter of 100 m positioned at a distance of 30 km from each other. As can be seen from the figure, a maximum ratio $[O_3]/([NO] + [NO_2])$ equal to 10^3 can be reached. Thus, there exist AIR creation conditions under which the ozone-to-nitric-oxide concentration ratio in an ionized region will be the same as in the unperturbed natural stratosphere [1].

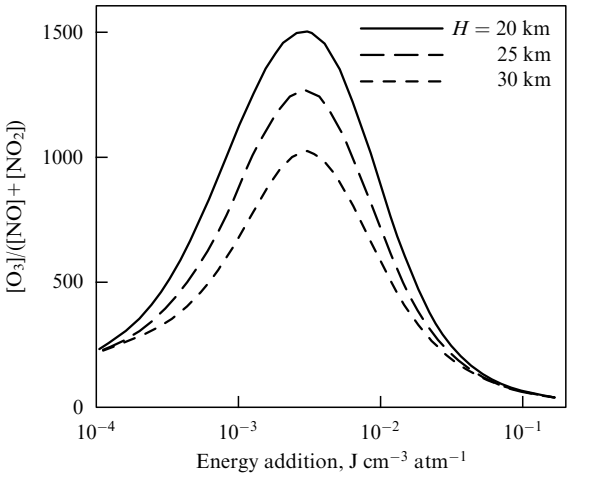

Figure 20. Ozone-to-nitric-oxide concentration ratio as a function of the specific energy addition to the AIR created by a single microwave pulse.

The existence of optimum energy additions to discharge plasma, for which the ratio [O_3]/[NO_x] is maximum, may be explained as follows. For low energy additions when the nitric oxide production is mainly determined by reaction (29), the process of atomic nitrogen fixation in the reverse reaction (30) causes an increase of the energy cost of nitric oxide generation [61]. As the energy addition to the system grows, the energy cost of NO_x production falls by virtue of switching to other NO_x production channels [reactions (17) and (32)], which results in a decrease of the ratio [O_3]/[NO_x] as well.

4.5 Remote diagnostics of plasma-chemical processes in an AIR

It is quite natural that an environmental experiment is to be provided with various type diagnostics for measuring ozone concentrations and other minor constituents. As is well known, the ozone layer is now being continuously monitored [63]. Ozone in the upper atmosphere is examined with devices measuring the total ozone content and with lidar ozonometers [64]. These diagnostics are also quite suitable for the experiment under discussion. For ozone diagnostics it is reasonable to apply remote methods and laser-based apparatus that provide the possibility of obtaining operative information with high space-time resolution [65, 66]. The use of lasers also makes it possible to determine the concentrations of some minor constituents of the atmosphere, which cannot be measured by other techniques. The ozone concentration distribution in the stratosphere can be obtained with good spatial resolution with the help of a UV lidar using an XeCl laser (e.g., with wavelengths of 307.9 and 308.2 nm) [65]. Scattered radiation is detected in the photon counting regime.

Paper [67] is devoted to remote diagnostics of minor atmospheric components and discusses the method for measuring concentrations of various impurities in the atmosphere using the AIR. Ionization in an AIR is accompanied by atomic and molecular excitation by electron impact. The concentration of atoms of sort s in an excited electron state j can be found from the relationships

$$\frac{dN_{js}}{dt} = k_{js} N_e(t) N_s - \frac{N_{js}}{\tau_{js}}, \tag{51}$$

$$N_e(t) = N_{e0} \exp(\nu_i t), \tag{52}$$

where k_{js} is the excitation coefficient for the corresponding atom, $k_{js} = f[f(v), \omega, P]$, τ_{js} is the lifetime of the electronically excited state, $\nu_i = k_i N_m$ is the ionization frequency, and N_s and N_m are respectively the number densities of sort s

impurity and air at the AIR altitude. From these two equations one finds the number P_{js} of photons emitted from this excited state. Photons are received by a telescope of area S, positioned at a distance Z from the microwave breakdown region. Within the microwave pulse time τ their number is equal to

$$P_{js} = \frac{k_{js}}{k_{\rm i}} \frac{N_s}{N_{\rm m}} \frac{S}{4\pi Z^2} N_{\rm em} V, \tag{53}$$

where $N_{\rm em} = N_{\rm e}(t = \tau)$ is the electron density occurring within the microwave pulse time, and V is the AIR volume. This equation can be used to find the value of $N_s/N_{\rm m}$ because the ratio $k_{js}/k_{\rm i}$ for the case $\omega > \nu$ is a readily determinable quantity depending only on the oscillator energy $\epsilon_\sim$ of electrons and on the ratio between electron impact molecular excitation and ionization cross sections, $\sigma_{js}/\sigma_{\rm i}$ [15, 21, 67].

Two different methods for the determination of active particle number density were considered in Ref. [67]. The first method is based on passive spectroscopy and can be applied to determine the number density of particles that make allowed transitions in the optical range. Measurements of optical radiation intensity may help to determine the concentrations of atoms and molecules: Cl, ClO, CO, NO, H, N, O, and F.

The second method makes use of a differential absorption lidar. It is applicable to the determination of the number density of particles having metastable electronic states excited by electron impacts. The number of metastables is found using two laser pulses with slightly different wavelengths through comparison of their light absorptions. The first laser wavelength is chosen to correspond to strong absorption in the transition between the metastable level and the optically allowed level positioned above the metastable one. The second laser wavelength is chosen on the wing of the absorption curve. This method helps to measure the CO, NO, OH, and H atomic and molecular concentrations. The calculations made in Ref. [67] showed that for the microwave radiation parameters $\lambda = 3$ cm, $P = 4$ GW, $\tau = 100$ ns, and $F = 1$ kHz and for the antenna diameter of 34 m, the ratio $N_s/N_{\rm m}$ can be determined:

(1) by the first method at the level $N_s/N_{\rm m} \sim 10^{-11}$, where $\sim 10^3$ microwave pulses will be required for this, which corresponds to the accumulation time of 1 s for the pulse repetition frequency $F = 1$ kHz;

(2) by the second method, also at the level $N_s/N_{\rm m} \sim 10^{-11}$, where $\sim 10^4 - 10^5$ microwave pulses will be required for this, which corresponds to the accumulation time of 10 – 100 s for the same pulse repetition rate.

4.6 Formation of an artificial ozone layer

To observe an artificial ozone layer in a natural physical experiment and to measure the ozone concentration, a fairly vast region should be replenished with ozone. The discussed earlier antenna complex (see Fig. 1) can, for example, by scanning the beams, move their crossing region in space over an area of 100 km^2.

When an extensive region in the stratosphere is to be filled with ozone, atmospheric wind and turbulent diffusion may be of great help. The influence of these factors in the Chapman model with allowance for the wind unvaried in magnitude and direction and the diffusion in the horizontal plane was analyzed in paper [59]. We shall generalize here the results obtained in that paper by including the vertical diffusion and nitrogen components into the consideration.

Suppose that under the influence of a microwave discharge in the atmosphere the minor neutral components changed slightly as compared to their background values. Our goal is to describe the slow temporal and spatial variations of an artificially perturbed ozone concentration. In the equations we carry out time averaging over the interval of twenty four hours and express the concentrations of different components in terms of the ozone concentration to arrive at the following approximate equation (cf. Ref. [59])

$$\left[\frac{\partial}{\partial t} + v\frac{\partial}{\partial x} - D_1\left(\frac{\partial^2}{\partial x^2} + \frac{\partial^2}{\partial y^2}\right) - D_z\frac{\partial^2}{\partial z^2}\right]\delta[{\rm O}_3] = -\frac{\delta[{\rm O}]_3}{\tau_p} + Q_{\rm eff}. \tag{54}$$

Here, $\delta[{\rm O}_3]$ is the time average of an addition to the ozone concentration, v is the wind velocity, τ_p is the perturbation relaxation time, D_1 and D_z are horizontal and vertical turbulent diffusion coefficients, and $Q_{\rm eff}$ is the intensity of the effective ozone source. The coordinate axis x is aligned with the wind velocity, y lies in the horizontal plane and is orthogonal to x, and z is pointing vertically upward. Note that the effective-source intensity $Q_{\rm eff}$ is determined in our case not only by the rate of ozone production from atmospheric oxygen (with a plus sign), but also by the influence of the nitrogen catalytic cycle (with a minus sign).

The solution of equation (54) at a large distance from a lumped source has the form

$$\delta[{\rm O}_3] \approx \bar{Q}_{\rm eff}\frac{1}{4\pi\sqrt{D_1 D_z}x} \times \exp\left\{-\left[\frac{x}{v\tau_p} + \frac{v}{4D_1 x}\left(y^2 + z^2\frac{D_1}{D_z}\right)\right]\right\},$$

$$\bar{Q}_{\rm eff} = \int Q_{\rm eff}\,{\rm d}^3x. \tag{55}$$

From the latter equation it follows that the ozone layer is asymmetric: it is strongly elongated in the direction of the wind motion. The characteristic layer dimensions along the x-, y-, and z-axes are respectively equal to $L_x \approx v\tau_p$, $L_y \approx \sqrt{4D_1\tau_p}$, and $L_z \approx \sqrt{4D_z\tau_p}$. Thus, a strong wind and turbulent diffusion favor the spread of the perturbation over a vast spatial domain. The characteristic layer half-thickness $L_z/2 \approx \sqrt{D_z\tau_p}$ is determined by the vertical diffusion coefficient and the AIR lifetime. According to different authors, the coefficient D_z for the altitude $H = 18 - 20$ km varies over a wide range $2 \times 10^3 < D_z < 10^5$ cm^2 s^{-1} [1]. Assuming a lifetime $\tau_p \approx 100$ d, we evaluate the half-thickness of the artificial ozone layer as $0.27\ {\rm km} < L_z/2 < 1.9$ km. This implies that the thickness of the artificial ozone layer, even with allowance made for vertical diffusion, appears to be much smaller than that of the natural ozone layer. Estimating the horizontal diffusion coefficient $D_1 \sim 10^9$ cm^2 s^{-1} and the wind velocity $v \sim 10$ m s^{-1}, from formula (55) we obtain that over a period of about 100 d the area of the artificial ozone layer reaches $S \sim 10^7$ km^2, i.e. can even cover a region comparable with the Antarctic ozone hole.

The possibility of performing an environmental experiment also depends on the magnitude of necessary expenditure of energy. We shall estimate the mean power necessary to replenish a local region with ozone. Over an area $S = 10^3$ km^2,

ozone can be regenerated by a single microwave complex as shown in Fig. 1. The expenditure of energy can be minimized if the minimum necessary amount of ozone is generated. This minimum can be assessed considering ozone generation with a number density equal to the natural level $[O_3] = 2 \times 10^{12}$ cm^{-3} at an altitude of 18 km in a layer $\Delta H = 2$ km in thickness. The estimates show that an ozone layer that thick diminishes UV radiation at a wavelength of 250 nm by two orders of magnitude.

The mean power $\bar{P}$ required for ozone generation depends on the area S of the artificial ozone layer and on the characteristic time τ_p of ozone decomposition:

$$\bar{P} = [O_3]\Delta H S \frac{\eta}{\tau_p} . \quad (56)$$

The lifetime of regenerated ozone in a local region depends on the zonal wind velocity. At medium latitudes at an altitude of between 18 and 24 km, a layer always exists with a low wind velocity of the order of 0.1 – 1 m s^{-1} [1, 68]. With a such wind velocity and the area $S = 10^3$ km^2 of an artificial ozone layer, the characteristic time is $\tau_p \approx 10$ d. For a local ozone region, the power $\bar{P}$ specified by equation (56) for $\eta = 20$ eV, $[O_3] = 2 \times 10^{12}$ cm^{-3}, and $\Delta H = 2$ km is equal to 10^7 W.

5. Conclusions

At the present time, a cycle of experimental and theoretical studies has been accomplished, devoted to the elaboration of a natural physical experiment on the action on the stratosphere by high-power crossed electromagnetic wave beams with the goal of generating additional ozone in the region of the ozone layer. Thus, active sensing of the ozone layer (its state and the whole complex of proceeding photochemical processes) is planned by introducing a controlled considerable amount of additional ozone and creating a local artificial ozone layer. The workability of this method was analyzed on specially designed experimental complexes for laboratory simulation of plasma-chemical processes in an artificially ionized region created by nanosecond wave beams. The experiments were carried out with air pressures and temperatures corresponding to ozone layer altitudes. The possibility of using a nanosecond microwave discharge in wave beams for generation of ozone and other minor species in the stratosphere was demonstrated experimentally for the first time.

On the one hand, this circumstance may allow the efficient employment of various AIR regimes for experimental sensing and investigation of the effect of minor components upon the ozone layer. On the other hand, the results of simulation experiments and numerical calculations suggest the possibility of efficient artificial ozone generation in local regions of the stratosphere. To this end, at altitudes of about 20 – 25 km, AIRs should be formed by microwave radiation with 3-cm wavelength and an electric field strength between 4 and 6 kV cm^{-1} in the beam crossing region and a microwave pulse duration of 30 – 50 ns.

We shall list the main advantages of this scheme.

(1) When short pulses of nanosecond duration ($\tau = 30 - 50$ ns) are used, an artificial ozonizer in the stratosphere is able to produce 100 g of ozone per 1 kW · h of expended electric energy. Such an atmospheric ozonizer output corresponds to the results of the best ozonizers currently used for technological purposes.

(2) Ozone is generated directly at the maximum of the natural ozone layer. Its 'delivery' requires no expenditure of energy (radio waves have no weight!).

(3) The technique of localization and deliberate displacement of the ozone generation region in space is very simple.

(4) A wonderful gift of nature is the low temperature ($T \sim 200 - 220$ K) in the ozonizer operation region. Owing to this fact, an exceptionally small quantity of nitric oxides participating in the catalytic ozone-decomposing processes are produced in nanosecond pulses. The latter circumstance is decisive for ensuring the high stratospheric ozonizer efficiency. Under these conditions, the energy cost of ozone production is moderate (15 – 20 eV per molecule in experiments, and 30 – 40 eV per molecule in calculations).

(5) The highest ozone generation efficiency is attained with the use of microwave pulses for which the breakdown stage is much shorter than the pulse duration subject to the condition that the circular frequency of the electromagnetic field is lower than the electron – molecule collision frequency ($\omega < \nu_c$). In this case, the majority of the microwave pulse energy is absorbed in the discharge plasma. It is of no less importance that in a wide range of regimes the values of the specific energy addition to the system are simultaneously reached for which nitric oxide generation becomes insignificant because the ratio $[O_3]/([NO] + [NO_2])$ is equal to or exceeds 10^3.

(6) An optimum regime of application to the atmosphere is a small train of nanosecond pulses and a subsequent change of the AIR location through scanning by the wave beams.

(7) Owing to atmospheric winds, turbulent diffusion, and the long (over 100 d) lifetimes of ozone molecules at the altitudes of the ozone layer maximum and lower, the ozone generated in an AIR spreads over large distances and can create a rather extensive local artificial ozone layer.

(8) The above-listed properties, as well as the possibility of moving the ozone generation region in the stratosphere over large distances (tens of kilometers) from ground-based oscillators of high-power electromagnetic waves make it possible to weaken considerably the ecological consequences of high-power microwave radiation by placing 'ozonizers' in special remote regions.

The analysis of the technological feasibility of an environmental experiment shows that the current state of engineering has reached the necessary level. Antennas 50 – 60 m in diameter are available, and they are the most costly units of the whole complex. Not relativistic microwave oscillators, but relatively low-power (and therefore inexpensive) microwave radiation sources (magnetrons of power below 1 MW) endowed with microwave pulse compression facilities and widely used in active pulsed radar may be employed in the natural physical experiment. Microwave pulse compressors yielding output pulses with a power of the order of 100 MW are being intensively designed [69 – 72]. Consequently, several such sources (not more than 50) will provide the necessary power level in one wave beam. The average power of such a microwave complex will make up 0.1 – 1 MW.

Thus, the series of theoretical studies and laboratory experiments discussed here demonstrate that it is in principle possible to generate ozone in the stratosphere using an AIR. The estimates show that owing to the long ozone lifetime at stratospheric altitudes (18 – 20 km), winds, and turbulent diffusion, the ozone generated in local regions spreads over large distances and may initiate artificial ozonization over global-scale regions. At the same time we should emphasize

that the difficulties (energetic, economical, ecological, and technological) associated with a global change of the ozone layer are obvious. Their discussion now seems untimely, although some attempts have already been made [73]. To clarify the situation, it is necessary to carry out a demonstrative environmental experiment. Notice that the environmental experiment under discussion will not lead to any significant global disturbances, but will undoubtedly provide a deeper insight into the complex plasma-chemical processes in the ozone layer. Only after this experimentation will a somewhat realistic estimation of the global program become feasible.

It should be noted that not only AIR-based ozone generation in the atmosphere is discussed in the scientific literature. The AIR creation in the lower atmosphere (troposphere) for removal of Freons from the atmosphere was proposed by G A Askar'yan et al. [74, 75] in the early 1990s. Within this project, an AIR was mainly considered as a source of electrons, and therefore provision was made for the use of short nanosecond microwave pulses with which the air ionization consumes the greater fraction of the microwave energy [19]. After a microwave pulse, at the stage of plasma decay, cold electrons selectively decompose Freon molecules owing to the high rate of electron dissociative attachment and then the chlorine-containing compounds fall to the ground with the rain. The cross sections of the dissociative attachment of electrons to, say, Freon-11 ($CFCl_3$) and Freon-12 (CF_2Cl_2) molecules possess maxima for low electron energies ($T_e \leqslant 0.06$ eV) [76], whereas for the electron dissociative attachment to oxygen molecules the energy threshold is 4 eV. This fact provides for the selectivity of the effect of cold electrons on Freons.

In the troposphere, for a low Freon number density ($\sim 10^9$ cm^{-3}) [1] and a high air pressure, the electron dissociative attachment frequency to Freon molecules turns out to be much lower than the three-body electron attachment frequency to oxygen molecules, and therefore the number of decomposed Freon molecules depends on the electron concentration in the plasma by the moment of microwave pulse termination and on the rate of plasma decay. The model proposed in Refs [74, 75] assumed a slow recombinative decay of plasma in the air, reached for relatively high specific energy additions to the plasma [28]. However, as was shown by the experimental studies of the decay of a nanosecond microwave discharge plasma in the air [77], a substantial fraction of the electrons produced are lost at the early stage of decay as a result of the three-body electron attachment to oxygen molecules. Upon the observed plasma decay, the Freon decomposition efficiency at altitudes of 18 – 20 km will be approximately an order of magnitude lower than that upon the electron – ion recombinative decay. The rates of plasma decay may in principle be decreased by increasing the pulse duration (i.e. the specific energy addition to the plasma), but this will lead to a negative ecological effect because the AIR will then be an efficient source of nitric oxides [22]. That is why, to clean low-density Freons out of the atmosphere, the microwave method should be further developed, but it is promising for Freon decomposition [78] or modification [79] inside industrial workshops on the ground for a high Freon molecule concentration in the air.

This work was performed under the sponsorship of the Russian Foundation for Basic Research (project #96-02-19467).

References

1. Brasseur G, Solomon S *Aeronomy of the Middle Atmosphere* (Dordrecht: D. Reidel Publ. Co., 1986) [Translated into Russian (Leningrad: Gidrometeoizdat, 1987)]
2. Aleksandrov E L et al. *Ozonnyĭ Shchit Zemli i Ego Izmeneniya* (The Ozone Shield of the Earth and its Evolution) (Leningrad: Gidrometeoizdat, 1992)
3. Danilov A D, Karol' I L *Atmosfernyĭ Ozon — Sensatsii i Real'nost'* (Atmospheric Ozone: Sensations and Reality) (Leningrad: Gidrometeoizdat, 1991)
4. Stalarski R S *Sci. Am.* **258** (1) 20 (1988) [*V Mire Nauki* (3) 6 (1988)]
5. Toon O B, Turco R P *Sci. Am.* **264** (6) 40 (1991) [*V Mire Nauki* (8) 34 (1991)]
6. Johnston H S *Science* **173** 517 (1971)
7. *Propulsion Effluents in Stratosphere* (CIAP. Monograph 2) (DOT-TST-75-52, Washington, DC, 1975)
8. Farman J C, Gardner B G, Shanklin J D *Nature* (London) **315** 207 (1985)
9. Flyagin V A et al. *IEEE Trans. Microwave Theory Techniques* **MTT-25** 514 (1977)
10. Gaponov-Grekhov A V, Petelin M I *Vestn. Akad. Nauk SSSR* (4) 11 (1979)
11. Bollen W M et al. *J. Appl. Phys.* **54** 101 (1983)
12. Armstrong W T et al., in *Proc. 18th Intern. Conf. on Phenomena in Ionized Gases* Vol. 4 (Ed. W T Williams) (Swansea, UK: Adam Hilger, 1987) p. 850
13. Vikharev A L et al. *Zh. Eksp. Teor. Fiz.* **94** (4) 136 (1988) [*Sov. Phys. JETP* **67** 724 (1988)]
14. Kuo S P, Zhang Y S *Phys. Fluids B* **2** 667 (1990)
15. Tsang K et al. *Radio Sci.* **26** 1345 (1991)
16. Vikharev A L et al., in *Vysokochastotnyĭ Razryad v Volnovykh Polyakh* (Microwave Discharge in Wave Fields) (Ed. A G Litvak) (Gor'kiĭ: IPF AN SSSR, 1988) p. 41
17. Karfidov D M, Lukina N A, Sergeĭchev K F *Fiz. Plazmy* **7** 312 (1981) [*Sov. J. Plasma Phys.* **7** 168 (1981)]
18. Gurevich A V et al. *Geomagn. Aeron.* **20** 953 (1980)
19. Gurevich A V *Usp. Fiz. Nauk* **132** 685 (1980) [*Sov. Phys. Usp.* **23** 862 (1980)]
20. Borisov N D, Gurevich A V, Milikh G M *Iskusstvennaya Ionizirovannaya Oblast' v Atmosfere* (An Artificially Ionized Region in Atmosphere) (Moscow: IZMIRAN, 1986)
21. Gurevich A V, Borisov N D, Milikh G M *Physics of Microwave Discharges*: *Artificially Ionized Regions in the Atmosphere* (Amsterdam: Gordon and Breach, 1997)
22. Askar'yan G A et al. *Dokl. Akad. Nauk SSSR* **302** 566 (1988); *Fiz. Plasmy* **17** 85 (1991) [*Sov. J. Plasma Phys.* **17** 48 (1991)]
23. Borisov N D, Kozlov S I, Smirnova N V *Kosmich. Issled.* **31** (2) 63 (1993) [*Cosmic Res.* **31** 177 (1993)]
24. Milikh G M *J. Geophys. Res. D* **95** 16451 (1990)
25. Larin V F *Pis'ma Zh. Tekh. Fiz.* **16** (8) 85 (1990) [*Sov. Tech. Phys. Lett.* **16** 319 (1990)]
26. Eliasson B, Kogelschatz U *IEEE Trans. Plasma Sci.* **19** 1063 (1991)
27. Vikharev A L et al. *Fiz. Plazmy* **10** 165 (1984) [*Sov. J. Plasma Phys.* **10** 96 (1984)]
28. Vikharev A L, Ivanov O A, Stepanov A N *Fiz. Plazmy* **10** 792 (1984) [*Sov. J. Plasma Phys.* **10** 460 (1984)]
29. Vikharev A L et al. *Izv. Vyssh. Uchebn. Zaved. Radiofiz.* **30** 317 (1987)
30. Gil'denburg V B, Kim A V *Zh. Eksp. Teor. Fiz.* **74** 141 (1978) [*Sov. Phys. JETP* **47** 72 (1978)]
31. Gil'denburg V B, Kim A V *Fiz. Plazmy* **6** 904 (1980) [*Sov. J. Plasma Phys.* **6** 496 (1980)]
32. Borisov N D, Gurevich A V *Geomagn. Aeron.* **20** 841 (1980)
33. Borisov N D, Gel'fond O A, Gurevich A V *Fiz. Plazmy* **9** 1047 (1983) [*Sov. J. Plasma Phys.* **9** 610 (1983)]
34. Borisov N D *Fiz. Plazmy* **8** 712 (1982) [*Sov. J. Plasma Phys.* **8** 401 (1982)]
35. Kochelap V A, Izmailov I A, Mel'nikov L Yu *Chem. Phys. Lett.* **157** (1 – 2) 67 (1989)
36. Vikharev A L et al., in *Proc. 21st Intern. Conf. on Phenomena in Ionized Gases* Vol. 1 (Eds G Ecker, U Arendt, J Boseler) (Bochum: APP, 1993) p. 123

37. Vikharev A L et al. *Phys. Lett. A* **179** 122 (1993)
38. Vikharev A L et al. *J. Geophys. Res. D* **99** 21097 (1994)
39. Akhmedzhanov R A et al. *Pis'ma Zh. Tekh. Fiz.* **21** (9) 26 (1995) [*Tech. Phys. Lett.* **21** 327 (1995)]
40. Akhmedzhanov R A et al. *Phys. Lett. A* **207** 209 (1995)
41. Akhmedzhanov R A et al. *Zh. Tekh. Fiz.* **67** (3) 9 (1997) [*Tech. Phys.* **42** 260 (1997)]
42. Vikharev A L, Ivanov O A, Litvak A G *IEEE Trans. Plasma Sci.* **24** 460 (1996)
43. Baulch D L et al. *J. Phys. Chem. Ref. Data* **11** 327 (1982)
44. Atkinson R et al. *J. Phys. Chem. Ref. Data* **18** 881 (1989)
45. Krivonosova O E et al., in *Khimiya Plazmy* (Plasma Chemistry) Vol. 14 (Ed. B M Smirnov) (Moscow: Energoatomizdat, 1987) p. 3
46. Zhivotov V K, Rusanov V D, Fridman A A *Diagnostika Neravnovesnoĭ Khimicheski Aktivnoĭ Plazmy* (Diagnostics of Nonequilibrium Chemically Active Plasma) (Moscow: Energoatomizdat, 1985)
47. Zhivotov V K, Rusanov V D, Fridman A A, in *Khimiya Plazmy* (Plasma Chemistry) Vol. 11 (Ed. B M Smirnov) (Moscow: Energoatomizdat, 1984) p. 200
48. Akhmedzhanov R A et al. *Fiz. Plazmy* **23** 58 (1997) [*Plasma Phys. Rep.* **23** 53 (1997)]
49. Eliasson B, Hirth M, Kogelschatz U *J. Phys. D* **20** 1421 (1987)
50. Eliasson B, Kogelschatz U, Research Report KLR 86-11C (Baden: Brown Boveri, 1986)
51. Bykov Yu V *Khim. Vys. Energ.* **18** 347 (1984)
52. Gurevich A V et al. *Phys. Lett. A* **201** 234 (1995); Lukina N A, Sergeichev K F, Sychov I A, in *Proc. 21st Intern. Conf. on Phenomena in Ionized Gases* Vol. 1 (Eds G Ecker, U Arendt, J Boseler) (Bochum: APP, 1993) p. 83
53. Aleksandrov N L et al. *Teplofiz. Vys. Temp.* **19** 485 (1981)
54. MacDonald A D *Microwave Breakdown in Gases* (New York: Wiley, 1966) [Translated into Russian (Moscow: Mir, 1969)]
55. Samoĭlovich V G, Gibalov V I, Kozlov K V *Fizicheskaya Khimiya Bar'ernogo Razryada* (Physical Chemistry of Barrier Discharge) (Moscow: Izd. Mosk. Gos. Univ., 1989)
56. Aleksandrov N L, Konchakov A M *Pis'ma Zh. Tekh. Fiz.* **16** (6) 4 (1990) [*Sov. Tech. Phys. Lett.* **16** 206 (1990)]
57. Molina M J, Rowland F S *Nature* (London) **249** 810 (1974)
58. Rowland F S, Molina M J *J. Phys. Chem.* **80** 2049 (1976)
59. Gurevich A V et al. *Phys. Lett. A* **207** 281 (1995)
60. Karol' I L, Kiselev A A, Frol'kis V A *Izv. Ross. Akad. Nauk Ser. Fiz. Atm. Okeana* **31** 120 (1995) [*Izv. Atm. Oceanic Phys.* **31** 113 (1995)]
61. Matveyev A A, Silakov V P *Phys. Rev. E* **54** 4121 (1996)
62. Vikharev A L, Ivanov O A, Litvak A G, in *Proc. Int. Workshop*: *Strong Microwaves in Plasmas* Vol. 1 (Ed. A G Litvak) (Nizhniĭ Novgorod: IAP Publ., 1997) p. 251
63. Margitan J J et al. *J. Geophys. Res. D* **100** 9193 (1995)
64. McGee T J et al. *J. Geophys. Res. D* **100** 9255 (1995)
65. Zakharov V M (Ed.) *Primenenie Lazerov dlya Opredeleniya Sostava Atmosfery* (The Use of Lasers for Determining Atmosphere Composition) (Leningrad: Gidrometeoizdat, 1983)
66. Measures R M *Laser Remote Sensing*: *Fundamentals and Applications* (New York: Wiley, 1984) [Translated into Russian (Moscow: Mir, 1987)]
67. Papadopoulos K et al. *J. Geophys. Res. D* **99** 10387 (1994)
68. Miles T et al. *J. Atm. Sci.* **51** 677 (1994)
69. Didenko A N, Yushkov Yu G *Moshchnye SVCh-Impul'sy Nanosekundnoĭ Dlitel'nosti* (Powerful Microwave Pulses of Nanosecond Duration) (Moscow: Energoatomizdat, 1984)
70. Didenko A N et al. *Dokl. Akad. Nauk SSSR* **321** (3) 518 (1991) [*Sov. Phys. Dokl.* **36** 792 (1991)]
71. Vikharev A L, Kovalev N F, Petelin M I *Pis'ma Zh. Tekh. Fiz.* **22** (19) 41 (1996) [*Tech. Phys. Lett.* **22** 795 (1996)]
72. Vikharev A L et al., in *Proc. Int. Workshop*: *Strong Microwaves in Plasmas* Vol. 2 (Ed. A G Litvak) (Nizhniĭ Novgorod: IAP Publ., 2000) p. 896
73. Batanov G M et al. *Fiz. Plazmy* **22** 1046 (1996) [*Plasma Phys. Rep.* **22** 580 (1996)]
74. Askar'yan G A et al. *Pis'ma Zh. Eksp. Teor. Fiz.* **55** 500 (1992) [*JETP Lett.* **55** 515 (1992)]; *Fiz. Plazmy* **18** 1198 (1992) [*Sov. J. Plasma Phys.* **18** 625 (1992)]
75. Askaryan G A et al. *J. Phys. D* **27** 1311 (1994)
76. Christophorou L G, Pinnaduwage L A *IEEE Trans. Electrical Insulation* **25** (1) 55 (1990)
77. Vikharev A L et al. *Zh. Tekh. Fiz.* **66** (7) 56 (1996) [*Tech. Phys.* **41** 665 (1996)]
78. Nusinovich G S, Milikh G M, Levush B *J. Appl. Phys.* **80** 4189 (1996)
79. Gritsinin S I et al. *Fiz. Plazmy* **23** 264 (1997) [*Plasma Phys. Rep.* **23** 242 (1997)]